Author Manuscript

Author Manuscript

Author Manuscript

Author Manuscript

HHS Public Access

Author manuscript

Nat Biomed Eng. Author manuscript; available in PMC 2023 January 01.

Published in final edited form as:

Nat Biomed Eng. 2022 January ; 6(1): 54–66. doi:10.1038/s41551-021-00740-x.

Inhibition of aberrant tissue remodelling by mesenchymal stromal cells singly coated with soft gels presenting defined chemomechanical cues

Sing Wan Wong[1,2], **Chandramohan R. Tamatam**[3,6], **Ik Sung Cho**[1,2,6], **Peter T Toth**[1,4], **Raymond Bargi**[1,2], **Patrick Belvitch**[5], **James C. Lee**[2], **Jalees Rehman**[1], **Sekhar P. Reddy**[3], **Jae-Won Shin**[1,2]

[1]Department of Pharmacology and Regenerative Medicine, University of Illinois at Chicago, Chicago, IL, USA.

[2]Department of Bioengineering, University of Illinois at Chicago, Chicago, IL, USA.

[3]Division of Developmental Biology and Basic Research, Department of Pediatrics, University of Illinois at Chicago, Chicago, IL, USA.

[4]Fluorescence Imaging Core, Research Resources Center, University of Illinois at Chicago, Chicago, IL, USA.

[5]Division of Pulmonary, Critical Care, Sleep and Allergy, Department of Medicine, University of Illinois at Chicago, Chicago, IL, USA.

[6]These authors contributed equally: Chandramohan R. Tamatam, Ik Sung Cho.

Abstract

The precise understanding and control of microenvironmental cues could be used to optimize the efficacy of cell therapeutics. Here, we show that mesenchymal stromal cells (MSCs) singly coated with a soft conformal gel presenting defined chemomechanical cues promote matrix remodelling by secreting soluble interstitial collagenases in response to the presence of tumour necrosis factor alpha (TNF-α). In mice with fibrotic lung injury, treatment with the coated MSCs maintained normal collagen levels, fibre density and microelasticity in lung tissue, and the continuous presentation of recombinant TNF-α in the gel facilitated the reversal of aberrant tissue

Correspondence and requests for materials should be addressed to J.-W.S. shinjw@uic.edu.

Author contributions

Conceptualization, S.W.W. and J.-W.S.; data curation, S.W.W. and J.-W.S.; formal analysis, S.W.W. and J.-W.S.; funding acquisition, J.-W.S. and S.P.R.; investigation, S.W.W., I.S.C., C.R.T., P.T.T., R.B. and P.B.; methodology, S.W.W., I.S.C., C.R.T., P.T.T., P.B., S.P.R. and J.-W.S.; project administration, J.-W.S.; resources, J.C.L., J.R., S.P.R. and J.-W.S.; software, S.W.W.; supervision, J.-W.S.; validation, S.W.W., I.S.C., C.R.T., R.B. and J.-W.S.; visualization, S.W.W., P.T.T. and J.-W.S.; writing original draft, S.W.W. and J.-W.S.; editing original draft, S.W.W., J.R., S.P.R. and J.-W.S.

Competing interests

The authors declare no competing interests.

Additional information

Supplementary information The online version contains supplementary material available at https://doi.org/10.1038/s41551-021-00740-x.

Peer review information *Nature Biomedical Engineering* thanks James Ankrum, Matthew Dalby and Jeffrey Spees for their contribution to the peer review of this work.

Reprints and permissions information is available at www.nature.com/reprints.

Author Manuscript Author Manuscript Author Manuscript Author Manuscript

remodelling by the cells when inflammation subsided in the host. Gel coatings with predefined chemomechanical cues could be used to tailor cells with specific mechanisms of action for desired therapeutic outcomes.

Tissue injury activates inflammation, which is followed by remodelling, the process broadly defined as reorganization of tissues[1]. In some disease conditions, remodelling processes become aberrant, resulting in irreversible tissue fibrosis[2]. Aberrant tissue remodelling often results in physical changes in the extracellular matrix (ECM), which impair physiological tissue mechanics, leading to persistent organ dysfunction[3,4]. Pathological changes in tissue mechanics can be attributed to dysregulated production, degradation or post-translational modification of the ECM[5]. Most existing therapeutic strategies against fibrosis are designed to indirectly impact the ECM turnover by targeting cytokine or growth factor-mediated signalling pathways, but these approaches have resulted in only modest clinical improvements[6]. Thus, there is a need for strategies to directly modulate the ECM turnover that could either promote normal remodelling or even reverse aberrant remodelling after fibrotic tissue injury.

Treatment with mesenchymal stromal cells (MSCs) has been tested in many clinical trials and has demonstrated favourable safety profiles[7,8]. A number of studies have tested MSC-based treatment of fibrotic tissue injury[9–11]. So far, most of these studies have attributed the therapeutic efficacy of MSCs to the paracrine release of anti-inflammatory or immunomodulatory factors that are upregulated in response to inflammatory activation as an adaptive countermeasure[12,13]. However, this approach requires an inflammatory milieu in the host, which is present during the early phases of the disease[14]; this milieu is probably resolved by the time fibrosis is diagnosed and MSC-based therapies are considered. In addition, suppression of inflammation alone is insufficient to improve long-term outcomes in patients with lung fibrosis[15].

In principle, MSCs can regulate the ECM turnover by responding to both chemical and mechanical signals from their microenvironments[16–19], since MSCs in situ are normally present in interstitial regions surrounded by the ECM. For instance, MSCs increase degradation of the ECM in a pro-inflammatory cytokine milieu by secreting some isoforms of matrix metalloproteinases (MMPs)[20], but MSCs also synthesize more collagen molecules in response to ECM stiffening[21,22]. However, it remains unclear how microenvironmental cues can be precisely harnessed to control the ECM turnover in a regulated manner that can be used to direct MSCs to resolve fibrotic injury. More broadly, there is a need for technologies to tailor MSC-based therapeutics with specific chemomechanical cues for desired outcomes.

Encapsulating cells in engineered matrices before delivery allows the presentation of precisely defined chemomechanical cues[23]. In particular, encapsulation of individual therapeutic cells into microscale hydrogels facilitates delivery of both cells and materials into deep tissues without major surgery[24]. Previous studies have shown that microencapsulation of donor cells improves therapeutic outcomes in some disease models by delaying clearance[25] or preventing host rejection[26,27]. However, it remains unclear whether microencapsulation can be leveraged to locally specify chemomechanical cues

Author Manuscript Author Manuscript Author Manuscript Author Manuscript

around donor cells to improve their therapeutic efficacy. Here we present an approach where chemomechanical cues are defined to direct the MSC secretome to promote matrix remodelling, and are subsequently packaged into conformal gel coating to encapsulate individual donor MSCs for delivery to tissues that undergo aberrant tissue remodelling upon fibrotic injury (Fig. 1a).

Results

Soft matrix enhances soluble interstitial collagenase production in MSCs by TNF-α.

We tested the central hypothesis that MSCs respond to specific inflammatory and matrix biophysical signals, and subsequently correct aberrant tissue remodelling processes via the release of paracrine factors. Here we focused on MMPs, which regulate a number of fundamental processes involving normal and aberrant tissue remodelling[17,28]. Tumour necrosis factor alpha (TNF-α), interferon-γ (IFN-γ), interleukin-1β (IL-1β) and lipopolysaccharide (LPS) were first tested as inflammatory signals since they have been previously implicated in eliciting anti-inflammatory and therapeutic functions of MSCs as an adaptive response to injury[29]. Clonally derived marrow D1 mouse MSCs were chosen for initial studies since clonal populations provide greater cell-to-cell homogeneity than primary cells[30]. TNF-α upregulated mRNA expression of soluble interstitial collagenases, including *Mmp13* (Fig. 1b, left) and *Mmp1a* (Fig. 1b, right), to a greater extent than other tested inflammatory signals. In contrast, TNF-α did not substantially upregulate gelatinases (for example, *Mmp2*) (Supplementary Fig. 1a). We next assessed whether primary mouse and human bone marrow MSCs would show similar effects and found upregulation of collagenases in these cells upon activation by inflammatory signals (Supplementary Fig. 1b,c). Thus, TNF-α is a prominent inducer of soluble interstitial collagenase expression in MSCs.

To identify downstream signalling pathways that mediate TNF-α-induced upregulation of soluble interstitial collagenases, we tested *Mmp13* mRNA expression in response to TNF-α in the presence of inhibitors against p38 mitogen-activated protein kinase (MAPK), c-Jun N-terminal kinase (JNK) and extracellular signal-regulated kinase 1/2 (ERK1/2) pathways —SB203580 (10 μM), SP600125 (20 μM) and U0126 (5 μM), respectively. Inhibition of p38 MAPK and JNK but not inhibition of ERK1/2 suppressed TNF-α-induced upregulation of *Mmp13* mRNA (Fig. 1c, left). In contrast, only inhibition of p38 MAPK was able to reduce IL^{-1}β-induced upregulation of *Mmp13* mRNA (Fig. 1c, right), suggesting that JNK is selective to TNF-α-induced upregulation of *Mmp13* mRNA. TNF-α induced phosphorylation of JNK isoforms p46 (at Thr183) and p54 (at Tyr185) in 20 min to a greater extent than IL-1β, while both TNF-α and IL-1β induced phosphorylation of p38 MAPK at Thr180 and Tyr 182 to a similar extent (Fig. 1d). These results suggest that the JNK pathway plays an important role in TNF-α-induced *Mmp13* expression.

We then sought to better understand the impact of patho-physiologically relevant mechanical cues on the ability of MSCs to express MMPs in response to TNF-α. To address this question, we used a synthetic alginate (LF200, ~240 kPa, 1% weight per volume (w/v)) hydrogel system conjugated with the minimal integrin adhesion ligand Arg-Gly-Asp (RGD) (~60 μM; Supplementary Fig. 2a) with tunable stiffness (Young's modulus, *E*) (alginate-

Author Manuscript Author Manuscript Author Manuscript Author Manuscript

RGD) (Supplementary Fig. 2b)[31]. Most D1 mouse MSCs remained viable 3 days after encapsulation in soft ($E \approx 2$ kPa) or stiff ($E \approx 20$ kPa) bulk gels (Supplementary Fig. 2c). Hydrogel stiffness did not impact the diffusion of TNF-α recombinant protein into the gels (Supplementary Fig. 2d). To characterize the effect of hydrogel stiffness on TNF-α-induced expression of collagenases, dose–response studies were performed. The soft bulk gel increased the maximum response of TNF-α to upregulate *Mmp13* (Fig. 1e, left) and *Mmp1a* (Fig. 1e, right) mRNA by ~1.9-fold and ~3-fold, respectively. Primary mouse and human bone marrow MSCs also showed similar effects upon treatment with TNF-α after encapsulation in bulk gels (Supplementary Fig. 2e,f). In addition, the soft bulk gel reduced the dose of TNF-α required for the half-maximum response (that is, it increased potency) to upregulate *Mmp13* and *Mmp1a* mRNA by ~4.5-fold and ~1.3-fold, respectively (Fig. 1e). Consistently, TNF-α-induced phosphorylation of JNK was higher when MSCs were encapsulated in the soft bulk gel than in the stiff bulk gel (Fig. 1f). Thus, TNF-α and soft matrix constitute chemomechanical cues that enhance the production of soluble interstitial collagenases by MSCs.

Gel coating enables MSCs to degrade collagen over distance in response to TNF-α.

We tested the possibility that MSCs treated with TNF-α in soft matrix can be leveraged to degrade collagen in a paracrine manner, which can potentially be useful to control remodelling processes that result in tissue rigidification by collagen deposition or crosslinking[32]. We leveraged a droplet microfluidic approach to miniaturize the soft bulk alginate-RGD gel into conformal gel coating of individual cells (μMSC; Fig. 2a(i)). To facilitate delivery to tissues with a narrow space, such as small airways, we further tuned the approach to minimize the volume of gel coating by two to roughly three times that of a single MSC (Fig. 2a(ii)) while maintaining soft E at ~2 kPa (Fig. 2a(iii)). This approach yielded gel-coated viable MSCs (Fig. 2a(iv)) with high efficiency without the need to perform additional cell sorting, and is thus suited for therapeutic uses. A high-molecular-weight alginate (~240 kDa) was chosen to keep most MSCs from proliferating[33,34], as confirmed by a low level of 5-ethynyl-2′deoxyuridine (EdU) incorporation for 1 day, as opposed to MSCs in collagen-I gel (Fig. 2a(v)). Importantly, gel coating keeps MSCs from adopting myofibroblast phenotypes for at least 3 days after encapsulation, since the gene expression of α-smooth muscle actin (*Acta2*), beta-actin (*Actb*) and tumour growth factor-β1 (*Tgfβ1*) remained lower than that of MSCs in the stiff bulk gel, consistent with a previous study[35]—*Tgfβ1* expression was even lower in gel-coated MSCs than MSCs in the soft bulk gel (Supplementary Fig. 3a).

TNF-α-induced expression of collagenases in gel-coated MSCs was then tested. Despite the similar diffusion kinetics of TNF-α into the microgel versus the bulk gel with the same $E \approx 2$ kPa (Supplementary Fig. 3b), gel coating of single D1 mouse MSCs resulted in approximately threefold higher TNF-α-induced upregulation of *Mmp13* and *Mmp1a* than bulk gel encapsulation of MSCs (Fig. 2b). Treatment of gel-coated MSCs with TNF-α increased collagenase activity in the conditioned media, which was further enhanced by approximately twofold when the media were treated with the saturating concentration (1 mM) of 4-aminophenylmercuric acetate (APMA), the chemical activator of latent MMPs[36] (Fig. 2c). Primary mouse and human bone marrow MSCs also showed similar effects upon

Author Manuscript Author Manuscript Author Manuscript Author Manuscript

treatment with TNF-α after gel coating (Supplementary Fig. 3c–e). Thus, gel-coated MSCs secrete both active and latent forms of collagenases in response to TNF-α. Gel-coated D1 mouse MSCs were capable of degrading the surrounding collagen-I ex vivo upon activation with TNF-α for 1 day in culture in an MMP-dependent manner, since incubation with the pan-MMP inhibitor GM6001 (10 μM) suppressed this process (Fig. 2d(i–ii)). Most MSCs remained within the microgels (Fig. 2d(iii)), suggesting that gel-coated MSCs can degrade collagen-I in a paracrine manner. Thus, gel coating is an enabling cue for MSCs to degrade collagen over distance by producing soluble collagenases in response to TNF-α.

Gel coating enables MSCs to promote normal remodelling after fibrotic lung injury in vivo.

To investigate the therapeutic relevance of our results, we tested the hypothesis that gel coating enables MSCs to inhibit tissue rigidification induced by fibrotic injury during acute host inflammation. A bleomycin-induced injury model was used to test the hypothesis, since it has been leveraged to reproducibly recapitulate some aspects of aberrant tissue remodelling, including enhanced collagen production and crosslinking[37]. The lungs were chosen as the model organ of interest, since they are frequently exposed to exogenous injury, which could lead to scar formation in interstitial regions, thereby compromising respiration[38]. Lung fibrosis is also a terminal disease for afflicted patients due to the lack of efficacious therapies[6]. To this end, we instilled bleomycin (0.015 U per 20 g mouse) intratracheally (i.t.) to induce injury in the mouse lungs. The basal total collagen level in the lungs was ~0.3 μg hydroxyproline per mg tissue. After bleomycin treatment, this value remained at the baseline at week 1 but increased by approximately twofold to ~0.6 μg mg^{-1} at week 2 (Supplementary Fig. 4a(i)). Infiltration of neutrophils, lymphocytes and macrophages into the airways also increased and peaked 2 weeks after bleomycin treatment, suggesting a high level of inflammation (Supplementary Fig. 4a(ii–iv)).

To test whether gel coating enables MSCs to suppress excess collagen deposition, 100,000 gel-coated D1 mouse MSCs were delivered i.t. per 20 g mouse after 1 week of bleomycin treatment, followed by analyses after 1 week of cell delivery (Fig. 3a). Gel-coated MSCs, but not uncoated MSCs, significantly limited total hydroxyproline deposition to ~0.45 μg mg^{-1} in the lungs (Fig. 3b). Automated analyses of Masson's trichrome-stained lung sections based on machine learning[39] (Supplementary Fig. 4b,c) showed decreased fibrotic mass and increased maintenance of normal alveoli after delivery of gel-coated MSCs compared with other tested groups (Fig. 3c). Three-dimensional (3D) two-photon analyses of fresh lung samples[40] showed that only gel-coated MSCs significantly reduce accumulation of fibrillar collagen in the lung parenchyma (Fig. 3d). To test whether gel-coated MSCs also preserve physiological lung tissue stiffness against bleomycin treatment, we used atomic force microscopy (AFM) to measure microelasticity of lung parenchymal sections[22,41]. Gel-coated MSCs, but not uncoated MSCs, significantly reduced lung tissue stiffness by ~threefold compared with the vehicle control (Fig. 3e). Gel-coated MSCs were effective in reducing infiltration of neutrophils and lymphocytes into the airways, while macrophage infiltration remained unchanged (Fig. 3f). We next assessed the MSC dose required for achieving therapeutic efficacy and found that lower doses of gel-coated MSCs were not effective (Supplementary Fig. 5a), thus suggesting that 100,000 gel-coated MSCs per 20 g mouse is probably the minimum effective dose in this context. Increasing the dose

Author Manuscript Author Manuscript Author Manuscript Author Manuscript

of uncoated MSCs to 500,000 cells per 20 g mouse was not sufficient to recapitulate the effect of gel-coated MSCs (Supplementary Fig. 5b). The gel alone was not bioactive, since empty alginate-RGD microgels (~20 μm in diameter) that did not contain cells showed no significant effect when delivered via either i.t. or intravenous (i.v.) route (Supplementary Fig. 5c). Gel coating of primary mouse bone marrow MSCs also resulted in reduced levels of collagen deposition, reduced accumulation of fibrillar collagen in the lung parenchyma and infiltration of neutrophils and lymphocytes—these effects were observed in both i.t. (Supplementary Fig. 6a) and i.v. (Supplementary Fig. 6b) routes of delivery. Gel-coated primary MSCs were also able to reduce infiltration of macrophages upon i.t. delivery (Supplementary Fig. 6a(v)). Thus, gel coating of MSCs is an effective means of suppressing fibrotic lung injury while minimizing the number of required therapeutic donor cells.

Delivery routes determine the effect of gel coating on the residence time of MSCs.

To test whether the ability of gel-coated MSCs to inhibit fibrotic lung injury can be attributed to the increased residence time of MSCs, we used D1 mouse MSCs that express firefly luciferase to track their biodistribution kinetics in vivo. Both i.v. and i.t. routes led to localization of MSCs in the lung regions of the mice previously treated with bleomycin for 1 week, within 30 min of administration. Consistent with the previous results[42], i.v. injected, uncoated MSCs were rapidly cleared from the lungs (half-life, $t_{1/2} \approx 5$ h) with no evidence of subsequent integration in other tissues. Gel coating significantly increased the residence time of i.v. injected MSCs by ~3.5-fold ($t_{1/2} \approx 18$ h) and enhanced the remaining fraction of MSCs by ~2-fold in 7 days (Supplementary Fig. 7a). In contrast, i.t. delivered, uncoated MSCs were cleared slower than i.v. injected, uncoated MSCs by ~3-fold ($t_{1/2} \approx 15$ h)—despite this, uncoated MSCs did not significantly inhibit bleomycin-induced lung injury (Fig. 3). Gel coating did not delay the clearance of i.t. delivered MSCs (Supplementary Fig. 7b) in terms of half-life, plateau and total area of the biodistribution curve (Supplementary Fig. 7c–e), thereby suggesting that the effect of gel coating on the residence time of MSCs depends on route of administration. Thus, the ability of gel-coated MSCs to suppress fibrotic lung injury was not due to increased residence time of MSCs.

Donor MMP13 and host TNF-α determine the efficacy of gel-coated MSCs in fibrotic injury.

We tested whether soluble collagenase from gel-coated D1 mouse MSCs contributes to their efficacy in bleomycin-induced lung injury. *Mmp13* was chosen as a soluble interstitial collagenase of interest for mechanistic studies, because its expression level is generally much higher than another isoform *Mmp1a* (Fig. 1 and Supplementary Fig. 1). D1 mouse MSCs were treated with *Mmp13* small interfering RNA (siRNA) or scrambled siRNA before gel coating. Transfection of siRNA in MSCs led to ~70% knockdown of *Mmp13* in 1 day compared with scrambled siRNA (Supplementary Fig. 8a). Gel-coated MSCs treated with *Mmp13* siRNA were no longer able to ameliorate hydroxyproline deposition compared with those treated with scrambled siRNA (Fig. 4a). The reduction of both neutrophils and lymphocytes by gel-coated MSCs was also no longer seen with *Mmp13* siRNA, suggesting that MMP13 suppresses recruitment of these cells into the lung airways (Fig. 4b). Therefore, MMP13 from donor MSCs is essential for gel-coated MSCs to suppress fibrotic lung injury.

Author Manuscript Author Manuscript Author Manuscript Author Manuscript

We next tested whether gel-coated MSCs require host TNF-α to suppress aberrant tissue remodelling in bleomycin-induced lung injury. The total collagen level in the lungs of *Tnfa*$^{-/-}$ mice was increased approximately twofold after 1 week of bleomycin treatment (Fig. 4c), just like in wild-type mice (Fig. 3b). However, gel-coated MSCs were no longer able to inhibit hydroxyproline deposition in the bleomycin-treated *Tnfa*$^{-/-}$ mice (Fig. 4c). Gel-coated MSCs also failed to reduce neutrophil infiltration in these mice, but they could still reduce lymphocyte infiltration independently of TNF-α (Fig. 4d). Treating with recombinant TNF-α before administration rescued the ability of gel-coated MSCs to reduce hydroxyproline deposition and neutrophil infiltration in *Tnfa*$^{-/-}$ mice (Fig. 4c,d). Together, the results show that both host TNF-α and donor MMP13 are required for the ability of gel-coated MSCs to ameliorate fibrotic lung injury.

Predicting the efficacy of MSCs delivered at different time points after fibrotic lung injury.

We developed a mathematical model to gain quantitative insights into how MSCs influence collagen deposition when delivered at different time points upon tissue injury (Supplementary Text). In this model, both maximum production rate (β_{mmp}) and dose response of TNF-α binding to MSCs ($\theta_{tnf\text{-}\alpha}$) determine collagenase secretion from MSCs, while a classical Michaelis–Menten equation describes collagen degradation kinetics by collagenases (δ_{col}) (Fig. 5a). Parameter values were set to recapitulate the phenotypes known to be induced by instillation of single-dose bleomycin—TNF-α in the airways is transiently increased to maximum at week 1, followed by a decrease over 5 weeks[43], while tissue collagen is increased to maximum between weeks 2 and 4, and later decreases at week 6[44] (Supplementary Fig. 8b). The model shows that increasing β_{mmp} as achieved by gel coating is sufficient to inhibit collagen deposition when MSCs are delivered 1 week after bleomycin treatment— setting β_{mmp} to 1.2 and 0.4 recapitulates the experimental results from delivering gel-coated MSCs and uncoated MSCs, respectively (Fig. 5b). After 3 weeks of bleomycin treatment when collagen deposition peaks, the host TNF-α level becomes lower from the maximum by 2.5-fold (Supplementary Fig. 8b)—when MSCs are delivered at this time point, the model suggests that both gel-coated (β_{mmp} = 1.2) and uncoated (β_{mmp} = 0.4) MSCs will not be as effective in resolving established collagen (Fig. 5c). When the host TNF-α level is restored to the maximum, however, the model predicts that gel-coated MSCs will resolve collagen deposition more substantially than uncoated MSCs when delivered at week 3 (Fig. 5c). The sensitivity analysis indicates that increasing β_{mmp} will decrease the half-maximum TNF-α concentration necessary to resolve collagen (Fig. 5d). Thus, the model predicts the importance of both gel coating and reconstituting TNF-α in enabling MSCs to facilitate normal tissue remodelling or reverse aberrant remodelling of injured tissues.

Gel-coated MSCs loaded with TNF-α facilitate the resolution of fibrotic phenotypes.

We next sought to develop a strategy to reverse aberrant tissue remodelling at later time points when fibrosis has set in and inflammation has already subsided. Approximately 10% of total recombinant mouse TNF-α protein was stably incorporated in alginate microgels for at least 3 days after incubation with the solution containing TNF-α for 1 day, followed by washing out unbound TNF-α (Supplementary Fig. 9a). This strategy was used to continuously present MSCs with recombinant TNF-α in gel coating and to test their efficacy

Author Manuscript Author Manuscript Author Manuscript Author Manuscript

in restoring injured tissues after aberrant remodelling by administering to mice 3 weeks after bleomycin treatment (Fig. 6a). Consistent with the model (Fig. 5), only gel-coated, TNF-α-loaded MSCs significantly reduced established collagen to ~0.4 μg mg^{-1} 1 week after delivery (Fig. 6b). In addition, gel-coated, TNF-α-loaded MSCs significantly reduced fibrotic mass, restored normal alveoli (Fig. 6c) and brought fibrillar collagen in the lung parenchyma to the physiological level (Fig. 6d). Gel-coated, TNF-α-loaded MSCs were also effective in restoring lung tissue closer to the physiological stiffness compared with other groups (Fig. 6e). Gel-coated, TNF-α-loaded MSCs accelerated the resolution of neutrophil and lymphocyte infiltrations, while macrophage infiltration remained unchanged (Fig. 6f).

To test whether TNF-α or MMP13 is sufficient to resolve fibrotic phenotypes, we loaded alginate-RGD microgels (~20 μm in diameter) with either recombinant mouse TNF-α or catalytically active mouse MMP13 proteins. The diffusion kinetics of TNF-α into microgels was fast ($t_{1/2}$ ≈ 0.46 h; Supplementary Fig. 3b), while that of MMP13 from microgels was an order of magnitude slower ($t_{1/2}$ ≈ 4 h; Supplementary Fig. 9b(i)). This feature provided an opportunity to mimic TNF-α-loaded, gel-coated MSCs by loading TNF-α briefly (~30 min) after the formation of microgels pre-loaded with MMP13, while still allowing microgels to continuously release MMP13 as they were administered in mice. The amount of MMP13 pre-loaded to microgels was chosen so that the maximum level of MMP13 released per microgel would be similar to the maximum level of MMP13 secreted per cell from TNF-α-treated, gel-coated MSCs (~5 fg per cell; Supplementary Fig. 9b(i)). The conditioned medium from MMP13-containing microgels, after release for 1 day, showed an equivalent collagenase activity (Supplementary Fig. 9b(ii)) to the medium from TNF-α-treated, gel-coated MSCs treated with 1 mM APMA (Fig. 2c). However, i.t. administration of 100,000 protein-loaded microgels per 20 g mice after 3 weeks of bleomycin treatment failed to reduce collagen deposition (Supplementary Fig. 9c(i)) or immune cell infiltration in the airways (Supplementary Fig. 9c(ii–iv)). Thus, TNF-α or MMP13-loaded microgels alone are not sufficient to resolve fibrotic injury. Together, specifically defined chemomechanical cues enable MSCs to accelerate the resolution of fibrotic phenotypes as predicted by the mathematical model.

Discussion

Success in some cell-based therapeutics depends on both fundamental understanding of how microenvironmental properties impact cellular functions and development of approaches to control these properties around donor cells. In this study, we show an approach where engineered gel coating is leveraged to specify chemomechanical cues for donor MSCs as a means to augment their ability to treat aberrant tissue remodelling after fibrotic injury. Specifically, we provide experimental evidence that cell therapy can be rationally designed by defining both soluble and insoluble signals, which together enhance the production of interstitial collagenases by MSCs—conformal gel coating of individual MSCs can then be used to locally present these signals after tissue delivery. Mechanistic studies support a mathematical model that informs strategies to optimize the effect of MSCs when delivered in different stages of fibrotic injury.

Author Manuscript Author Manuscript Author Manuscript Author Manuscript

While previous studies tested therapeutic effects of MSCs from a standard plastic culture in animal models of fibrotic lung injury, they showed variable outcomes[9]. In fact, only two studies administered MSCs after at least 1 week[45,46]—consistent with these studies, we show that MSCs without gel coating show limited efficacy when delivered 1 week after bleomycin treatment. Our combined mathematical modelling and experimental approaches show that therapeutic efficacy of MSCs probably depends on a number of parameters, including the level of host TNF-α, sensitivity of donor cells to TNF-α–ligand binding, and the maximum production rate of soluble interstitial collagenases, all of which may have contributed to variable outcomes from previous studies. Our results show that engineered gel coating can be used to optimize these parameters to improve MSC-based therapeutics against fibrotic lung injury.

Our work demonstrates that soft matrix potentiates the ability of MSCs to respond to TNF-α, which results in increased downstream production of soluble interstitial collagenases by activating JNK. TNF-α-induced JNK activation is known to be mediated by TNF receptor- associated factor 2 (TRAF2)[47], which was isolated biochemically as a complex of TNF receptor 2 (TNFR2)[48]. Hydrogels present cells with cytokines in a matrix-bound form, thereby activating receptors that may be less potently engaged by ligands in a free-soluble form, such as TNFR2[49]. Hydrogel stiffness can potentially impact TNF-α-mediated activation of MSCs either by influencing ligand mobility[50], or regulating receptor activation[51] or internalization[52]. Miniaturing a bulk gel into thin gel coating reduces material-to-cell volume ratios, which may further influence cell membrane fluidity and mobility of receptors. Our results highlight the importance of biomaterial design in sensitizing the activation of MSCs by a specific inflammatory signal to promote normal tissue remodelling as an adaptive response.

Cells possess tactile mechanisms that enable them to interpret properties of the surrounding matrix and subsequently control its turnover[53]. Gel coating presents MSCs with tactile matrix signals without a need for cells to cross endothelial or epithelial barriers to contact the ECM in the interstitium, so that they can be poised to remodel the host matrix via paracrine secretions. This strategy is also suitable to control physical contact of donor cells with host tissues before repair or regeneration. To study the impact of specifically defined chemomechanical cues in vivo, we focused on using the gel formulation to keep cells within gel coating, which are then cleared by the host without engraftment. Gel coating can further be modified to tune gel degradation[54] or fast stress relaxation[55] properties, and to introduce additional chemical modifications for delayed clearance[56], followed by evaluation of their impact on both treating aberrant tissue remodelling and engraftment of donor cells to host tissues.

Bacterial collagenases have been clinically approved for Dupuytren's contracture[57] and Peyronie's disease[58], but their safety and clinical utility in aberrant tissue remodelling remain unclear, thus highlighting the importance of further developing tissue modelling therapies. Although we show that the donor MMP13 and the host TNF-α are necessary for gel-coated MSCs to inhibit fibrotic injury, delivering catalytically active MMP13 alone or together with TNF-α via microgels was not sufficient to resolve fibrosis. These results suggest the possibility that resolution of fibrosis requires not only degradation of the fibrotic

Author Manuscript Author Manuscript Author Manuscript Author Manuscript

matrix but also restoration of a healthy matrix. Gel-coated MSCs may thus exert a dual function by degrading the fibrotic matrix via soluble collagenases and contributing to the restoration of the matrix, for example, by providing nascent matrix molecules[59]. In addition, it is possible that more sustained degradation of the fibrotic matrix by controlled delivery of collagenases may be necessary to resolve fibrosis—one way to achieve this goal is by sulfation of alginate gels to mimic heparin sulfate[60] that is known to bind to a number of MMP isoforms[61]. In addition, understanding how MMPs from donor cells are delivered to the interstitium, as a function of routes of administration, will help refine the mathematical model to predict their efficacy in aberrant tissue remodelling of different organs. Together, our results suggest a feasible approach that leverages mechanomedicine to get closer to the goal of predictively programming cellular functions for desired therapeutic outcomes.

Methods

Cell culture.

Clonally derived D1 mouse MSCs of bone marrow origin were purchased from American Type Cell Culture (ATCC, CRL-12424). Primary mouse bone marrow MSCs were derived from C57BL/6 J mouse donors (Cyagen, MUBMX-01001, 8- to 10-week-old male; mD1: from year 2018, mD2: from year 2019, mD3: from year 2021). Primary human bone marrow MSCs were derived by plastic adherence of mononucleated cells from human bone marrow aspirate donors (Lonza, 1M-105; hD1: 28-year-old male, hD2: 34-year-old male, hD3: 30-year-old male, hD4: 33-year-old male). All cells were cultured at 37 °C in 5% CO_2. D1 and primary mouse MSCs were cultured in complete media composed of high-glucose Dulbecco's modified Eagle medium (DMEM; Thermo) supplemented with 10% volume/volume (v/v) foetal bovine serum (FBS; S11550, Atlanta Biologicals), 100 units per ml penicillin–100 μg ml^{-1} streptomycin and 2 mM GlutaMAX (Thermo). Human MSCs were cultured in α-minimal essential medium (αMEM; Thermo) supplemented with 20% v/v FBS, 100 units per ml penicillin–100 μg ml^{-1} streptomycin and 2 mM GlutaMAX. Cells were passaged when they reached ~80% confluence in a 175 cm^2 flask by detaching with trypsin-EDTA (Thermo). D1 mouse MSCs with passage number less than 13, primary mouse MSCs with passage number less than 10 and primary human MSCs with passage number less than 4 were used for this study.

Soluble inflammatory mediators.

The following soluble inflammatory mediators were used to stimulate cells and purchased from Peprotech: TNF-α (human: 300–01 A, murine: 315–01 A; 100 ng ml^{-1}), IFN-γ (human: 300–02, murine: 315–05; 100 ng ml^{-1}) and IL-1β (human: 200–01 B, murine: 211–11 B; 100 ng ml^{-1}). LPS (from *E. coli* O111:B4; 2,000 ng ml^{-1}) was purchased from Sigma (L2630).

Inhibitors of signalling pathways.

The following chemical inhibitors were used to inhibit signalling pathways while cells were stimulated with TNF-α or IL-1β for 3 days, and purchased from Cayman Chemical: SB203580 (13067, 10 μM) to inhibit p38 MAPK, SP600125 (10010466, 20 μM) to inhibit JNK, U0126 (70970, 5 μM) to inhibit ERK1/2. The stock solutions of the inhibitors were

Author Manuscript Author Manuscript Author Manuscript Author Manuscript

dissolved in dimethylsulfoxide (DMSO, Sigma) at 10 mM. DMSO (1:500 dilution, or 28 mM) was used as a control.

Alginate-RGD preparation.

Sodium alginate with ~240 kDa molecular weight (LF200) was purchased from FMC Biopolymer. An integrin-binding peptide consisting of Arg-Gly-Asp (GGGGRGDSP; Peptide 2.0) was covalently conjugated to alginate by 1-ethyl-dimethylaminopropyl (EDC) and *N*-hydroxysulfosuccinimide (Sulfo-NHS) (Thermo) chemistry with ~60 μM as described previously[62]. After conjugation, alginate-RGD was dialysed against decreasing concentrations of NaCl, charcoal-treated, filter-sterilized and lyophilized. Lyophilized alginate was stored in −20 °C and dissolved in DMEM within 1 week before experiments. The amount of RGD conjugated to alginate was quantified by the LavaPep kit (LP-022010, Gel Company) as described[63], which is based on a naturally occurring fluorescent compound that binds to lysine, arginine and histidine residues in peptides[64]. After reacting the compound with RGD standard solutions dissolved in unconjugated 1% w/v (41.7 μM) LF200 alginate and 1% w/v alginate-RGD samples for 1 h at 37 °C, fluorescent signals were acquired by FlexStation 3 (Molecular Devices) at excitation/emission = 540/630 nm. To visualize alginate gels by fluorescence, a small amount (final w/v = 0.025% or 2.085 μM) of 10/60 alginate (~120 kDa; FMC Biopolymer) coupled with lissamine rhodamine B ethylenediamine (Thermo) was added before gel formation.

Cell encapsulation in bulk alginate-RGD hydrogels.

Cells were resuspended in 1% w/v (41.7 μM) LF200 alginate-RGD in DMEM and rapidly mixed with calcium sulfate by syringes. Calcium sulfate (Sigma) with final concentrations of 10 or 30 mM was used to form the soft or stiff bulk hydrogel, respectively. The mixed solution was deposited between two glass plates with 1-mm thickness. After 1.5 h, hydrogels were punched into 5-mm-diameter discs and cultured in a 96-well glass bottom plate (P96G-1.5–5-F, MatTek) in the complete media.

Microfluidic device fabrication.

Microfluidic devices were fabricated using soft lithography. To develop a photoresist, SU-8 3025 (MicroChem) was deposited onto a silica wafer to a defined height and cured by ultraviolet light exposure through a transparency mask (CAD/Art Services) for patterning. Polydimethylsiloxane (PDMS) (Dow Corning) was then mixed with a crosslinker at a ratio of 10:1, degassed, poured and cured for at least 3 h at 65 °C. The cured PDMS was peeled off the wafer and bonded to a glass slide by oxygen-plasma treatment of both surfaces. Microfluidic channels were then treated with Aquapel (PPG Industries) and dried. Polyethylene tubing (inner diameter: 0.38 mm; outer diameter 1.09 mm) and 27 G × 1/2 needles were used to connect microfluidic channels to syringes (Becton Dickinson).

Single-cell encapsulation in alginate gel coating.

As described previously[33,34], $CaCO_3$ nanoparticles (CalEssence; 900 nm diameter) were resuspended in the complete DMEM and dispersed by sonication with Vibra Cell sonicator at 75% amplitude for 1 min. The nanoparticles were then centrifuged at 50*g* for 5 min

Author Manuscript Author Manuscript Author Manuscript Author Manuscript

to discard larger aggregates, followed by 1,000*g* for 5 min for collection. Purified $CaCO_3$ nanoparticles were resuspended at 6 mg ml^{-1} with serum-free DMEM media. Cells were then incubated with $CaCO_3$ at 1:1 by rotation at room temperature for 1 h. Excess $CaCO_3$ nanoparticles were then washed out by centrifugation. The aqueous phase was prepared by resuspending $CaCO_3$-coated cells in the buffer consisting of DMEM with 50 mM HEPES, 10% v/v FBS, 100 units per ml penicillin–100 μg ml^{-1} streptomycin at pH 7.4, and mixing cells with 1% w/v (41.7 μM) LF200 alginate-RGD solution. The oil phase consisted of fluorinated oil (HFE-7500; 3 M) with 13 mM perfluoropolyether (PFPE, Miller Stephenson) as a surfactant and 5.3 mM acetic acid (Thermo) as an initiator of Ca^{2+} release from $CaCO_3$. The aqueous and oil phases were injected into the droplet microfluidic device. The device with channel height of 15 μm and width of 20 μm was used. The flow rate of the aqueous phase was set to 1 μl min^{-1}, while the flow rate of the oil phase was set to 3 μl min^{-1}. Emulsion was collected every 20 min followed by 40 min rotation at room temperature. The emulsion was then broken by the addition of 453 mM 1H, 1H, 2H, 2H-perfluoroctanol (Alfa Aesar). Gel-coated cells were washed twice with serum-free DMEM before downstream experiments. Alginate-RGD microgels without cells (~20 μm in diameter) were synthesized by using the aqueous phase consisting of 1% w/v alginate-RGD solution mixed with 4.8 mg ml^{-1} $CaCO_3$.

Mechanical characterization of hydrogels by atomic force microscopy.

To determine Young's modulus (*E*) of bulk alginate hydrogels, a gel disc of 5 mm × 1 mm was first placed onto a PDMS mold on a glass slide and immersed in a drop of DMEM. To determine *E* of the alginate gel coating after single-cell encapsulation, gel-coated cells were immobilized on a glass side pre-coated with 0.1 mg ml^{-1} of poly-L-lysine for 2 h. The sample was then placed in an MFP3D-BIO system (Asylum Research) to perform indentation analysis with a silicon nitride cantilever with an 18° pyramidal tip (MLCT, Bruker). A spring constant of the cantilever was determined from thermal fluctuations at room temperature (80–100 mN m^{-1}) before each analysis. A fluorescent microscope was used to bring the cantilever to the gel coating surface. Indentation was then performed in contact mode with 500 nm force distance and 1 μm s^{-1} velocity until trigger voltage (0.5 V) was reached, followed by retraction. To calculate *E*, force-indentation curves were fitted to the Hertzian model and Poisson's ratio = 0.5 by using MFP-3D software (14.48.159, Asylum Research).

Characterization of TNF-α diffusion and retention in gels.

One soft or stiff bulk alginate gel disc (5 mm diameter × 1 mm height) or 100,000 soft alginate microgels (~20 μm diameter) without encapsulated cells were added to each well in a 96-well plate. To measure the extent of TNF-α diffusion into gels, each sample was incubated in Fluorobrite DMEM (Thermo) with 100 ng ml^{-1} murine TNF-α for 8 and 24 h, followed by washout with DMEM and digestion with alginate lyase. To measure the extent of TNF-α retention in gels, each sample was incubated with 100 ng ml^{-1} murine TNF-α for 24 h, followed by washout and incubation without TNF-α for 0, 24 and 72 h—at each time point, gels were washed and digested. Murine TNF-α enzyme-linked immunosorbent assay (ELISA kit, 900-K54, Peprotech) was used to quantify the amount of TNF-α in gel digests and total TNF-α input against the standard curve.

Author Manuscript Author Manuscript Author Manuscript Author Manuscript

Confocal imaging to measure cell and gel coating volumes.

Cells in gels were incubated with 2 μM calcein AM for 1 h to stain cytoplasm. Samples were then washed with Hank's balanced salt solution (HBSS) and maintained in Fluorobrite DMEM at 37 °C in 5% CO_2 during confocal imaging in the Zeiss LSM 770 system with a motorized stage and the 20×/0.8 M27 Plan-Apochromat objective. To analyse cell and gel volume, *z*-stack images were captured at excitation/emission of 495/515 nm and 560/580 nm, respectively, along 60–90 μm total depth at 0.77μm steps. Imaris (×64 9.3.0, Bitplane) was used to perform 3D reconstruction of images from each stack. Voxels were generated in red and green signals to represent gel and cytoplasm, respectively. Thresholding values were set automatically, showing variations less than 10% across all the images from different experiments.

Retrieval of cells from gels.

Cells in alginate gels were retrieved by digesting with 3.4 mg ml^{-1} alginate lyase (Sigma) at 37 °C for 30 min. Samples were then centrifuged at 846*g* for 5 min and washed twice with HBSS, followed by downstream analyses.

Cell viability analysis by flow cytometry.

Cells were added to the stain buffer consisting of HBSS with 2 μM calcein AM (Biotium) and 2 μM ethidium Homodimer-1 (Thermo) for 20 min. LSRFortessa (Becton Dickinson) was used to acquire fluorescence signals of samples, followed by analysis with the software Weasel (v.2.7.1; Chromocyte). Percent cell viability was calculated by dividing the number of $calcein^{+}$ $ethidium^{-}$ events by the total event number. In some cases, APC beads (CalibriteTM; Becton Dickinson) with a known number were added in each sample to calculate an absolute number of viable and dead cells.

Measurement of protein phosphorylation by intracellular flow cytometry.

D1 mouse MSCs (100,000 cells per sample) in suspension, soft or stiff alginate-RGD bulk gel were stimulated with either recombinant TNF-α or IL-1β (100 ng ml^{-1} each) for 20 min. For MSCs in suspension, the LIVE/DEAD fixable Alexa 405 violet dead cell stain (1:1,000 dilution L34955, Thermo) was added 10 min after stimulation. For MSCs in bulk gels, each gel was rapidly (~1 min) digested with 25 mM ethylenediaminetetraacetic acid (EDTA) with the violet dye in DMEM, followed by incubation of the digested solutions on ice for 7 min. Cells were then washed out with DMEM with 0.1% bovine serum albumin (BSA) and fixed with 4% w/v (1.34 M) paraformaldehyde in HBSS at room temperature for 10 min. After washing twice with HBSS/0.1% BSA, cells were stained with either phospho-p38 MAPK (Thr180/Tyr182) (clone: D3F9, 4511) or phospho-JNK (Thr183/Tyr185) (clone: 81E11, 4668) rabbit monoclonal antibody (both from Cell Signaling Technology) at 1:100 dilution in the staining buffer (HBSS/0.1% saponin/0.1% BSA) for 2 h at room temperature. The samples were then washed out once with the staining buffer and incubated with the secondary antibody (donkey anti-rabbit immunoglobulin-γ Alexa 546, A10040, Thermo) at 1:400 dilution for 40 min at room temperature, followed by washing out and resuspension in HBSS. Flow cytometry analysis was done using LSRFortessa (Becton Dickinson). The sample incubated with the isotype control (rabbit immunoglobulin G, DA1E, Cell Signaling

Author Manuscript Author Manuscript Author Manuscript Author Manuscript

Technology) was used as a negative control. Signals from live cell (Alexa 405 violet negative) fractions were used for analysis. Median fluorescence intensity values of Alexa 546 were then used to quantify phosphorylated proteins relative to unstimulated samples.

Gene expression analysis.

Cells were lysed with 1 ml of Trizol reagent (Thermo) for 10 min. Samples in Trizol were stored at −80 °C if not processed immediately up to 1 week. Chloroform (200 μl) was added per 1 ml of Trizol for phase separation. Samples were centrifuged for 15 min at 14,686*g* at 4 °C. The top layer containing RNA was collected into a new tube, and then precipitated with 250 μl of isopropanol and 250 μl of 0.8 M sodium citrate combined with 1.2 M sodium chloride for at least 15 min at 4 °C. Samples were then centrifuged at 14,686*g* for 15 min at 4 °C. The supernatant was removed and the precipitated RNA was washed with 75% v/v (12.8 M) ethanol (Thermo), followed by centrifugation for 5 min at 5,287*g* at 4 °C. After removing ethanol, purified RNA was resuspended in 15 μl of RNase-free water (Thermo). NanoDrop spectrophotometer (Thermo) was used to quantify RNA concentration and quality. Complementary DNA was obtained by reverse transcription using SuperScript-III reverse transcriptase (Thermo). For each sample, 50 ng complementary DNA was added to each well in triplicate, followed by the Power SYBR Green PCR Master Mix (Thermo) or Low ROX Forget-Me-Not EvaGreen quantitative PCR (qPCR) Master Mix (Biotium). qPCR was performed in the ViiA7 qPCR system (Thermo) with QuantStudio 6/7 software (v1.3). Relative gene expression was calculated using the $2^{-\Delta Ct}$ method by normalizing the cycle threshold (Ct) value of each target gene to that of the reference gene (mouse *Gapdh* or human *GAPDH*). Supplementary Table 1 shows the list of primers for qPCR.

Quantification of collagen degradation in vitro.

To test collagenase activity in the conditioned media, 50,000 gel-coated D1 mouse MSCs were cultured in 200 μl complete medium ±100 ng ml^{-1} murine TNF-α for 3 days at 37 °C. Each conditioned medium (100 μl) was then mixed with 100 μg ml^{-1} DQ-collagen type I (D12060, Thermo) that generates fluorescence upon degradation and incubated for 1 day at 37 °C ± 1 mM APMA (A9563, Sigma). Fluorescent signals were then acquired using a PHERAStar microplate reader (BMG LABTECH) with excitation/emission of 488/520 nm. To visualize collagen degradation relative to cells, gel-coated or uncoated D1 mouse MSCs were embedded in 1.25 mg ml^{-1} collagen-I matrix containing 100 μg ml^{-1} DQ-collagen and cultured in complete DMEM medium ± 100 ng ml^{-1} murine TNF-α overnight. 1 mM APMA was added to each sample to completely activate latent MMPs. In some samples, the pan-MMP inhibitor GM6001 (CC1010, EMD Millipore, 10 μM) was added to test whether collagen degradation is attributed to MMPs. The fluorescent signal from DQ-collagen degradation was captured using a Zeiss LSM 770 confocal microscope under 20×/0.8 M27 Plan-Apochromat objective at excitation/emission of 495/515 nm. *Z*-stack images were captured along 40 μm total depth at 0.77-μm steps. Imaris was used for 3D reconstruction of *z*-stack images, followed by quantification of total fluorescent volumes per field of view.

Author Manuscript Author Manuscript Author Manuscript Author Manuscript

Production of recombinant protein-loaded microgels.

The aqueous phase was prepared by mixing catalytically active recombinant mouse MMP13 protein (105–472aa, 46.5 kDa from *E. coli*, EP014660MO, Lifeome) in 1% w/v LF200 alginate-RGD solution with 4.8 mg ml^{-1} $CaCO_3$ to form MMP13-loaded microgels via the droplet microfluidic device as described above. The recombinant murine TNF-α protein was loaded to either empty or MMP13-loaded microgels by incubating 50 ng ml^{-1} TNF-α in DMEM with microgels for 30 min to load ~6 ng ml^{-1} TNF-α, since ~12.5% of TNF-α will be loaded in ~0.4 h as shown in Supplementary Fig. 3b. The amount of MMP13 protein released from microgels was quantified by incubating 50,000 MMP13-loaded microgels per 200 μl complete DMEM medium, followed by collecting the media at 4, 24 and 72 h. In parallel, 50,000 gel-coated MSCs per 200 μl complete DMEM medium were incubated at ±100 ng ml^{-1} murine TNF-α, and the media were collected at 24 and 72 h. Mouse MMP13 ELISA kit (E90099Mu, Lifeome) was used to quantify the amount of MMP13 protein per microgel or cell. Collagen degradation activity of the conditioned media from MMP13-loaded microgels was measured after incubating 50,000 gels per 200 μl media for 1 day by DQ-collagen assay as described above. MMP13 ELISA and DQ-collagen assays were used to titrate the initial amount of MMP13 mixed in the alginate-RGD solution so that the maximum amount of MMP13 released per microgel would be similar to the maximum amount of MMP13 protein released per TNF-α-treated, gel-coated D1 mouse MSC—this amount was determined to be 0.75 μg MMP13 protein per 200 μl alginate-RGD solution to achieve ~5 fg MMP13 released per microgel (Supplementary Fig. 9b).

Animal model of bleomycin-induced lung injury.

All animal experiments were performed in compliance with NIH and institutional guidelines approved by the ethical committee from the University of Illinois at Chicago (ACC number: 18–231). C57BL/6 J (000664) and B6;129S-*Tnf*^{tm1Gkl}/J (003008, *Tnfα*$^{-/-}$) mice were purchased from the Jackson Laboratory. Mice (8 to 12 weeks old) were anesthetized with ketamine/xylazine (50/5 mg per kg), followed by single dose i.t. administration of bleomycin (0.015U per 20 g mouse) as described previously[65]. Bleomycin was diluted in 30 μl PBS and instilled using a 100 μl pipette tip after exposing the laryngopharynx area of the anesthetized mice. Both nostrils were temporarily closed to facilitate liquid flow into the trachea. After 1 or 3 weeks of bleomycin administration, animals received a vehicle (sterile serum-free Fluorobrite DMEM), 100,000 uncoated MSCs, or 100,000 gel-coated MSCs in 30 μl Fluorobrite DMEM per 20 g mouse via the i.t. route as done with bleomycin, or through the i.v. route via retro-orbital injection with a 27 G syringe needle. After 1 week of cell delivery, animals were killed for downstream analyses.

Bronchoalveolar lavage.

PBS (1 ml, Thermo) with 2 mM EDTA (Sigma) was added through the trachea and withdrawn by syringe to collect bronchoalveolar lavage (BAL) fluid. The BAL fluid was centrifuged at 845*g* for 10 min at 4 °C. Isolated cells were resuspended in 500 μl of PBS with 2 mM EDTA. After counting the total cell number using a haemocytometer with 49 mM crystal violet (Sigma), 70 μl of cells were deposited onto a glass slide by the Cytospin centrifuge (Thermo) at 294*g* for 5 min. Kiwi Diff staining kit (9990700, Thermo) was used

Author Manuscript Author Manuscript Author Manuscript Author Manuscript

to stain cells on the slide, followed by counting the number of macrophages, lymphocytes and neutrophils.

Quantification of hydroxyproline.

Lung tissue from each mouse was weighed and homogenized in 1 ml of water. One hundred microlitres of homogenate was mixed with 100 μl of 12 M HCl and incubated at 120 °C for 3 h. An assay kit (MAK008, Sigma) was used to quantify hydroxyproline. Ten microlitres of the lysate was loaded per well in a 96-well plate and dried at 65 °C for 1.5 h. Chloramine T oxidative buffer (100 μl, Sigma) was then added to each well and incubated at room temperature for 5 min, after which 100 μl 4-(dimethylamino) benzaldehyde (Sigma) was added to each well and incubated for 1.5 h at 65 °C. Colorimetric signals were captured at 560 nm absorbance using a plate reader (PHERAstar 3.0, BMG LABTECH). The level of hydroxyproline was extrapolated by the standard curve and the total amount was then calibrated by the weight of the total tissue.

Histology with Masson's trichrome stain.

The lungs were perfused with PBS as described[65] to clear blood cells before histological analysis, followed by fixation in 2% w/v (0.67 M) paraformaldehyde (Sigma) in PBS for at least 48 h. Tissues were then embedded into paraffin blocks and sectioned using a microtome with 5 μm thickness. Slides with tissue sections were baked at 45 °C at least for 2 h and washed with xylene to remove paraffin, followed by rehydration with gradient ethanol: 100% v/v (17 M), 95% (16 M) and 75% (12.8 M). Rehydrated samples were then treated with preheated Bouin's solution (HT10132, Sigma) for 1 h, followed by Masson's trichrome staining using a kit (HT15, Sigma) based on the manufacturer's protocol. The stained slides were dehydrated by gradient ethanol: 75%, 95%, 100%, and then washed with xylene, mounted and dried for 24 h. The Aperio ImageScope system (Leica) was used to digitize histology slides. The Orbit Image Analysis software (version 3.15) was used to quantify histology images by machine learning as described[39]. The object training function was used to classify fibrotic versus normal mass at low magnification and fibrotic versus normal alveoli at high magnification. Ten representative regions from each normal and bleomycin-treated lung tissue section were used to train the software. The trained model was then applied to all of the samples for automated analysis.

Second harmonic imaging microscopy.

Imaging was done with second harmonic generation in the Ultima Multiphoton Microscope System (Bruker) to quantify collagen fibres and elastin in freshly isolated lung tissue as described[40]. The Chameleon Ultra II Two-Photon laser (860 nm) operating at 80 MHz was used to excite lung tissue. Collagen fibres were visualized by capturing backward scattering of second harmonic generation through a bandpass 430/24 nm filter. Elastin was visualized through a 582/22 nm filter. *Z*-stack images of collagen and elastin signals were acquired in parenchymal regions (defined as between 20 and 50 μm in depth from tissue surface) with 1 μm interval via Prairie View software (5.4, Bruker), followed by 3D reconstruction and quantification of total elastin volume (E_v) and collagen volume (C_v) by Imaris. The elastin-to-collagen volume ratio index was calculated as described[66]: $(E_v - C_v)/(E_v + C_v)$.

Author Manuscript Author Manuscript Author Manuscript Author Manuscript

Quantification of lung tissue microelasticity.

After perfusion of the lungs, 800 μl of the optimal cutting temperature compound was added through the trachea. The lungs were then frozen in 4-methyl butane chilled with dry ice and stored at −80 °C for no longer than 1 week. Tissue slices (15 μm) were sectioned with the HM525 NX Cryostat (Thermo) and stored at −20 °C for no longer than 24 h before analysis. After thawing tissue slices at room temperature for 10 min and rinsing them with PBS, AFM was performed to measure tissue microelasticity with 250 nm force distance and 0.5 μm s^{-1} tip velocity until trigger voltage (0.5 V) was reached.

RNA interference.

Small interfering RNAs were purchased from Thermo Fisher Scientific as follows: *Mmp13* (Assay ID: 155380, AM16708) and scrambled (Silencer negative control no. 1 siRNA, AM4611). siRNA (4 nM) was mixed with Lipofectamine RNAiMAX transfection reagent (Thermo) for 15 min in Opti-MEM (Thermo). The mixture was then applied to MSCs and cultured for 1 day before gel coating. qPCR was used to confirm the knockdown efficiency of each target gene compared with the scrambled control.

Establishing MSCs that express firefly luciferase.

To introduce firefly luciferase in D1 mouse MSCs, premade lentiviral particles containing mCherry-IRES-Firefly were purchased from the Mass General Hospital Vector Core. MSCs were incubated with viral particles for 2 days. Fluorescent MSCs were then isolated by fluorescence-activated cell sorting and expanded for further analysis.

Tracking biodistribution of MSCs in vivo.

One week after bleomycin treatment, uncoated or gel-coated firefly luciferase expressing D1 mouse MSCs were delivered via i.t. or i.v. routes. The mice were then i.v. injected with 200 μl of 15 mg ml^{-1} D-luciferin (Syd Labs) in PBS per 20 g mouse at different time points, followed by bioluminescence imaging with the IVIS Spectrum (PerkinElmer) within 10 min of D-luciferin injection to measure an average radiance (photons s^{-1} cm^{-2} sr^{-1}) in the lung region using the Living Image software (4.0, PerkinElmer).

Mathematical modelling.

A set of differential equations were constructed to predict the effect of uncoated or gel-coated MSCs on the total collagen level in lung tissue (Supplementary Text) and numerically solved by using the ode45 function in MATLAB (R2017a, MathWorks). To simulate the effect of cell delivery 1 week after bleomycin treatment, the following initial values were used: MSC_0 = 100,000 cells; $Bleo_0$ = 0.215 U kg^{-1}; TNF-α_0 = 0.49 ng ml^{-1}; MMP_0 = 432 pg ml^{-1}; Col_0 = 0.3 μg per mg tissue. To simulate the effect of cell delivery 3 weeks after bleomycin treatment, the following initial values were used: MSC_0 = 100,000 cells; $Bleo_0$ = 0.0056 U kg^{-1}; TNF-α_0 = 0.2 ng ml^{-1}; MMP_0 = 432 pg ml^{-1}; Col_0 = 0.6 μg per mg tissue.

Statistical analysis.

Statistics were performed as described in figure captions. All statistical analyses were performed using GraphPad Prism version 8.1.0. Unless otherwise noted, statistical

Author Manuscript Author Manuscript Author Manuscript Author Manuscript

comparisons were made by one-way analysis of variance (ANOVA) followed by Tukey's multiple comparisons test when standard deviations did not vary between test groups, and by one-way Welch ANOVA followed by Dunnett T3 multiple comparisons test when standard deviations were variable. All of the data from biological replicates show normal distribution based on the Shapiro–Wilk normality test. To compare the mean differences between groups that have been split on two independent variables, two-way ANOVA followed by Bonferroni's multiple comparisons test was used. *A P* value less than 0.05 established statistical significance.

Reporting Summary.

Further information on research design is available in the Nature Research Reporting Summary linked to this article.

Data availability

The main data supporting the results in this study are available within the paper and its Supplementary Information. The data reported in the figures are available as Supplementary Information. The raw and analysed datasets generated during the study are available for research purposes from the corresponding authors on reasonable request.

Code availability

The codes used to solve ordinary differential equations for the mathematical modelling of MSC-mediated collagen degradation are available as Supplementary Information.

Supplementary Material

Refer to Web version on PubMed Central for supplementary material.

Acknowledgements

We thank A. B. Malik and S. Lenzini (University of Illinois at Chicago) for critical reading of the manuscript and invaluable comments. This work made use of instruments in the Fluorescence Imaging Core (Research Resources Center, UIC). This work was supported by the National Institutes of Health grant nos. R01-HL141255 and R00-HL125884 (to J.-W.S.) and R01-GM124235 and R01-HL136946 (to S.P.R.).

References

1. Pinet K. & McLaughlin KA Mechanisms of physiological tissue remodelling in animals: manipulating tissue, organ and organism morphology. Dev. Biol 451, 134–145 (2019). [PubMed: 30974103]
2. Duffield JS, Lupher M, Thannickal VJ & Wynn TA Host responses in tissue repair and fibrosis. Annu. Rev. Pathol 8, 241–276 (2013). [PubMed: 23092186]
3. Anlas AA & Nelson CM Tissue mechanics regulates form, function and dysfunction. Curr. Opin. Cell Biol 54, 98–105 (2018). [PubMed: 29890398]
4. Tschumperlin DJ, Ligresti G, Hilscher MB & Shah VH Mechanosensing and fibrosis. J. Clin. Invest 128, 74–84 (2018). [PubMed: 29293092]
5. Theocharis AD, Skandalis SS, Gialeli C. & Karamanos NK Extracellular matrix structure. Adv. Drug Deliv. Rev 97, 4–27 (2016). [PubMed: 26562801]
6. Mora AL, Rojas M, Pardo A. & Selman M. Emerging therapies for idiopathic pulmonary fibrosis, a progressive age-related disease. Nat. Rev. Drug Discov 16, 755–772 (2017). [PubMed: 28983101]

Author Manuscript Author Manuscript Author Manuscript Author Manuscript

7. Bailey AM, Mendicino M. & Au P. An FDA perspective on preclinical development of cell-based regenerative medicine products. Nat. Biotechnol 32, 721–723 (2014). [PubMed: 25093890]
8. Ankrum JA, Ong JF & Karp JM Mesenchymal stem cells: immune evasive, not immune privileged. Nat. Biotechnol 32, 252–260 (2014). [PubMed: 24561556]
9. Srour N. & Thebaud B. Mesenchymal stromal cells in animal bleomycin pulmonary fibrosis models: a systematic review. Stem Cells Transl. Med 4, 1500–1510 (2015). [PubMed: 26494779]
10. Zhao L, Chen S, Shi X, Cao H. & Li L. A pooled analysis of mesenchymal stem cell-based therapy for liver disease. Stem Cell Res. Ther 9, 72 (2018). [PubMed: 29562935]
11. Jeong H. et al. Mesenchymal stem cell therapy for ischemic heart disease: systematic review and meta-analysis. Int. J. Stem Cells 11, 1–12 (2018). [PubMed: 29482311]
12. Ortiz LA et al. Interleukin-1 receptor antagonist mediates the anti-inflammatory and antifibrotic effect of mesenchymal stem cells during lung injury. Proc. Natl Acad. Sci. USA 104, 11002–11007 (2007). [PubMed: 17569781]
13. Lee RH et al. Intravenous hMSCs improve myocardial infarction in mice because cells embolized in lung are activated to secrete the anti-inflammatory protein TSG-6. Cell Stem Cell 5, 54–63 (2009). [PubMed: 19570514]
14. Wang Y, Chen X, Cao W. & Shi Y. Plasticity of mesenchymal stem cells in immunomodulation: pathological and therapeutic implications. Nat. Immunol 15, 1009–1016 (2014). [PubMed: 25329189]
15. Idiopathic Pulmonary Fibrosis Clinical Research Network et al. Prednisone, azathioprine and N-acetylcysteine for pulmonary fibrosis. N. Engl. J. Med 366, 1968–1977 (2012). [PubMed: 22607134]
16. Assis-Ribas T, Forni MF, Winnischofer SMB, Sogayar MC & Trombetta-Lima M. Extracellular matrix dynamics during mesenchymal stem cells differentiation. Dev. Biol 437, 63–74 (2018). [PubMed: 29544769]
17. Bonnans C, Chou J. & Werb Z. Remodelling the extracellular matrix in development and disease. Nat. Rev. Mol. Cell Biol 15, 786–801 (2014). [PubMed: 25415508]
18. Malik R, Lelkes PI & Cukierman E. Biomechanical and biochemical remodelling of stromal extracellular matrix in cancer. Trends Biotechnol. 33, 230–236 (2015). [PubMed: 25708906]
19. Lozito TP, Jackson WM, Nesti LJ & Tuan RS Human mesenchymal stem cells generate a distinct pericellular zone of MMP activities via binding of MMPs and secretion of high levels of TIMPs. Matrix Biol. 34, 132–143 (2014). [PubMed: 24140982]
20. Ries C. et al. MMP-2, MT1-MMP and TIMP-2 are essential for the invasive capacity of human mesenchymal stem cells: differential regulation by inflammatory cytokines. Blood 109, 4055–4063 (2007). [PubMed: 17197427]
21. Engler AJ, Sen S, Sweeney HL & Discher DE Matrix elasticity directs stem cell lineage specification. Cell 126, 677–689 (2006). [PubMed: 16923388]
22. Liu F. et al. Feedback amplification of fibrosis through matrix stiffening and COX-2 suppression. J. Cell Biol 190, 693–706 (2010). [PubMed: 20733059]
23. Shin JW & Mooney DJ Improving stem cell therapeutics with mechanobiology. Cell Stem Cell 18, 16–19 (2016). [PubMed: 26748752]
24. Desai T. & Shea LD Advances in islet encapsulation technologies. Nat. Rev. Drug Discov 16, 338–350 (2017). [PubMed: 28008169]
25. Mao AS et al. Programmable microencapsulation for enhanced mesenchymal stem cell persistence and immunomodulation. Proc. Natl Acad. Sci. USA 116, 15392–15397 (2019). [PubMed: 31311862]
26. Vegas AJ et al. Long-term glycemic control using polymer-encapsulated human stem cell-derived beta cells in immune-competent mice. Nat. Med 22, 306–311 (2016). [PubMed: 26808346]
27. Veiseh O. et al. Size - and shape-dependent foreign body immune response to materials implanted in rodents and non-human primates. Nat. Mater 14, 643–651 (2015). [PubMed: 25985456]
28. Loffek S, Schilling O. & Franzke CW Series “matrix metalloproteinases in lung health and disease”: biological role of matrix metalloproteinases: a critical balance. Eur. Respir. J 38, 191–208 (2011). [PubMed: 21177845]

Author Manuscript Author Manuscript Author Manuscript Author Manuscript

29. Le Blanc K. & Mougiakakos D. Multipotent mesenchymal stromal cells and the innate immune system. Nat. Rev. Immunol 12, 383–396 (2012). [PubMed: 22531326]
30. Mao AS, Shin JW & Mooney DJ Effects of substrate stiffness and cell–cell contact on mesenchymal stem cell differentiation. Biomaterials 98, 184–191 (2016). [PubMed: 27203745]
31. Lenzini S, Bargi R, Chung G. & Shin JW Matrix mechanics and water permeation regulate extracellular vesicle transport. Nat. Nanotechnol 15, 217–223 (2020). [PubMed: 32066904]
32. Holle AW et al. Cell–extracellular matrix mechanobiology: forceful tools and emerging needs for basic and translational research. Nano Lett. 18, 1–8 (2018). [PubMed: 29178811]
33. Mao AS et al. Deterministic encapsulation of single cells in thin tunable microgels for niche modelling and therapeutic delivery. Nat. Mater 16, 236–243 (2017). [PubMed: 27798621]
34. Wong SW et al. Controlled deposition of 3D matrices to direct single cell functions. Adv. Sci 7, 2001066 (2020).
35. Dingal PC et al. Fractal heterogeneity in minimal matrix models of scars modulates stiff-niche stem-cell responses via nuclear exit of a mechanorepressor. Nat. Mater 14, 951–960 (2015). [PubMed: 26168347]
36. Galazka G, Windsor LJ, Birkedal-Hansen H. & Engler JA APMA (4-aminophenylmercuric acetate) activation of stromelysin-1 involves protein interactions in addition to those with cysteine-75 in the propeptide. Biochemistry 35, 11221–11227 (1996). [PubMed: 8780527]
37. Liu T, De Los Santos FG & Phan SH The bleomycin model of pulmonary fibrosis. Methods Mol. Biol 1627, 27–42 (2017).
38. Thannickal VJ, Zhou Y, Gaggar A. & Duncan SR Fibrosis: ultimate and proximate causes. J. Clin. Invest 124, 4673–4677 (2014). [PubMed: 25365073]
39. Seger S. et al. A fully automated image analysis method to quantify lung fibrosis in the bleomycin-induced rat model. PLoS ONE 13, e0193057 (2018).
40. Pena AM et al. Three-dimensional investigation and scoring of extracellular matrix remodelling during lung fibrosis using multiphoton microscopy. Microsc. Res. Tech 70, 162–170 (2007). [PubMed: 17177275]
41. Liu F. et al. Distal vessel stiffening is an early and pivotal mechanobiological regulator of vascular remodelling and pulmonary hypertension. JCI Insight 10.1172/jci.insight.86987 (2016).
42. Parekkadan B. & Milwid JM Mesenchymal stem cells as therapeutics. Annu. Rev. Biomed. Eng 12, 87–117 (2010). [PubMed: 20415588]
43. Smith RE, Strieter RM, Phan SH, Lukacs N. & Kunkel SL TNF and IL-6 mediate MIP-1alpha expression in bleomycin-induced lung injury. J. Leukoc. Biol 64, 528–536 (1998). [PubMed: 9766634]
44. Redente EF et al. Tumor necrosis factor-alpha accelerates the resolution of established pulmonary fibrosis in mice by targeting profibrotic lung macrophages. Am. J. Respir. Cell Mol. Biol 50, 825–837 (2014). [PubMed: 24325577]
45. Ortiz LA et al. Mesenchymal stem cell engraftment in lung is enhanced in response to bleomycin exposure and ameliorates its fibrotic effects. Proc. Natl Acad. Sci. USA 100, 8407–8411 (2003). [PubMed: 12815096]
46. Huang K. et al. Conversion of bone marrow mesenchymal stem cells into type II alveolar epithelial cells reduces pulmonary fibrosis by decreasing oxidative stress in rats. Mol. Med. Rep 11, 1685–1692 (2015). [PubMed: 25411925]
47. Reinhard C, Shamoon B, Shyamala V. & Williams LT Tumor necrosis factor alpha-induced activation of c-jun N-terminal kinase is mediated by TRAF2. EMBO J. 16, 1080–1092 (1997). [PubMed: 9118946]
48. Rothe M, Wong SC, Henzel WJ & Goeddel DV A novel family of putative signal transducers associated with the cytoplasmic domain of the 75 kDa tumor necrosis factor receptor. Cell 78, 681–692 (1994). [PubMed: 8069916]
49. Grell M. et al. The transmembrane form of tumor necrosis factor is the prime activating ligand of the 80 kDa tumor necrosis factor receptor. Cell 83, 793–802 (1995). [PubMed: 8521496]
50. Huebsch N. et al. Harnessing traction-mediated manipulation of the cell/matrix interface to control stem-cell fate. Nat. Mater 9, 518–526 (2010). [PubMed: 20418863]

Author Manuscript Author Manuscript Author Manuscript Author Manuscript

51. Wong SW, Lenzini S, Cooper MH, Mooney DJ & Shin JW Soft extracellular matrix enhances inflammatory activation of mesenchymal stromal cells to induce monocyte production and trafficking. Sci. Adv 6, eaaw0158 (2020).
52. Du J. et al. Integrin activation and internalization on soft ECM as a mechanism of induction of stem cell differentiation by ECM elasticity. Proc. Natl Acad. Sci. USA 108, 9466–9471 (2011). [PubMed: 21593411]
53. Devine D. et al. Hydrogel micropost arrays with single post tunability to study cell volume and mechanotransduction. Adv. Biosyst 4, e2000012 (2020).
54. Khetan S. et al. Degradation-mediated cellular traction directs stem cell fate in covalently crosslinked three-dimensional hydrogels. Nat. Mater 12, 458–465 (2013). [PubMed: 23524375]
55. Chaudhuri O. et al. Hydrogels with tunable stress relaxation regulate stem cell fate and activity. Nat. Mater 15, 326–334 (2016). [PubMed: 26618884]
56. Rodriguez PL et al. Minimal “self” peptides that inhibit phagocytic clearance and enhance delivery of nanoparticles. Science 339, 971–975 (2013). [PubMed: 23430657]
57. Hurst LC et al. Injectable collagenase clostridium histolyticum for Dupuytren’s contracture. N. Engl. J. Med 361, 968–979 (2009). [PubMed: 19726771]
58. Gelbard M. et al. Clinical efficacy, safety and tolerability of collagenase clostridium histolyticum for the treatment of Peyronie disease in 2 large double-blind, randomized, placebo controlled phase 3 studies. J. Urol 190, 199–207 (2013). [PubMed: 23376148]
59. Loebel C, Mauck R. & Burdick JA Local nascent protein deposition and remodelling guide mesenchymal stromal cell mechanosensing and fate in three-dimensional hydrogels. Nat. Mater 10.1038/s41563-0190307-6 (2019).
60. Freeman I, Kedem A. & Cohen S. The effect of sulfation of alginate hydrogels on the specific binding and controlled release of heparin-binding proteins. Biomaterials 29, 3260–3268 (2008). [PubMed: 18462788]
61. Yu WH & Woessner JF Jr. Heparan sulfate proteoglycans as extracellular docking molecules for matrilysin (matrix metalloproteinase 7). J. Biol. Chem 275, 4183–4191 (2000). [PubMed: 10660581]
62. Rowley JA, Madlambayan G. & Mooney DJ Alginate hydrogels as synthetic extracellular matrix materials. Biomaterials 20, 45–53 (1999). [PubMed: 9916770]
63. Ingavle GC et al. Injectable mineralized microsphere-loaded composite hydrogels for bone repair in a sheep bone defect model. Biomaterials 197, 119–128 (2019). [PubMed: 30641263]
64. Bell PJ & Karuso P. Epicocconone, a novel fluorescent compound from the fungus Epicoccum nigrum. J. Am. Chem. Soc 125, 9304–9305 (2003). [PubMed: 12889954]
65. Rajasekaran S, Vaz M. & Reddy SP Fra-1/AP-1 transcription factor negatively regulates pulmonary fibrosis in vivo. PLoS ONE 7, e41611 (2012).
66. Lin SJ et al. Evaluating cutaneous photoaging by use of multiphoton fluorescence and second-harmonic generation microscopy. Opt. Lett 30, 2275–2277 (2005). [PubMed: 16190442]

Author Manuscript Author Manuscript Author Manuscript Author Manuscript

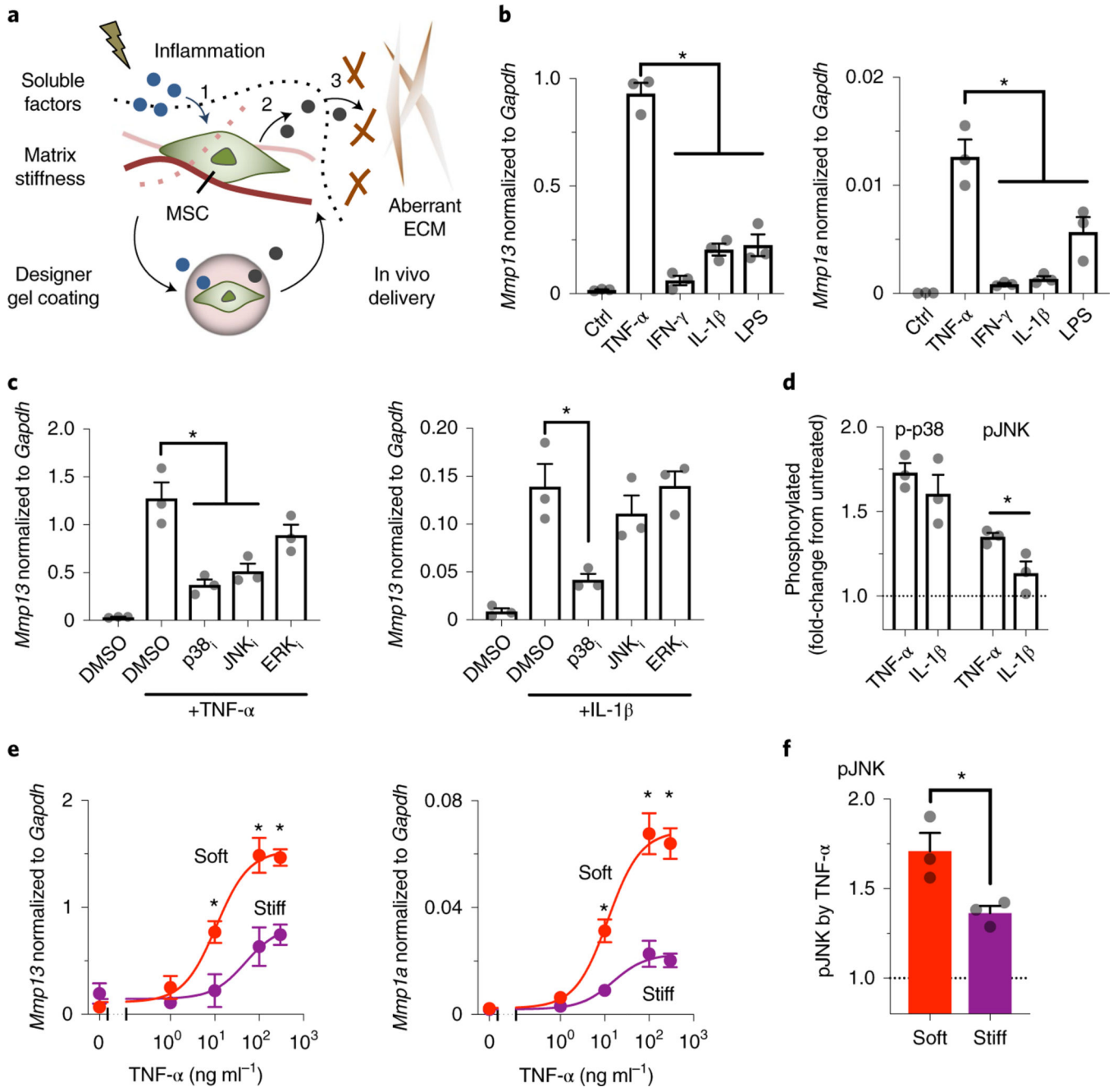

Fig. 1 |. Defining chemomechanical cues that enhance the production of soluble interstitial collagenases in mouse MSCs.

a, Tissue injury induces changes in both inflammatory and biophysical cues that influence the ability of MSCs to (1) accept soluble signals and (2) interpret them to produce paracrine factors. Gel coating can provide MSCs with predefined chemomechanical cues to optimize specific mechanisms of action, such as (3) correction of aberrant ECM remodelling. **b**, Left: effects of soluble inflammatory mediators on expression of *Mmp13*; and right: of *Mmp1a*, in D1 mouse MSCs treated for 3 days on plastic culture. TNF-α, IFN-γ and IL-1β were added at 100 ng ml^{-1}, while LPS was added at 2,000 ng ml^{-1}.Transcript levels are normalized to

Author Manuscript Author Manuscript Author Manuscript Author Manuscript

Gapdh. **P* = (1.4–2.9)×10^{-5} (left), *P* = (0.2–2.4) × 10^{-2} (right). Ctrl, control. **c**, Left: effects of inhibitors against signalling pathways on *Mmp13* expression induced by TNF-α; and right: by IL-1β, in D1 mouse MSCs treated for 3 days on plastic culture. $p38_i$, p38 MAPK inhibitor, SB203580 (10 μM); JNK_i, JNK inhibitor, SP600125 (20μM); ERK_i, ERK1/2 inhibitor, U0126 (5μM); **P* = (0.6–2.3) × 10^{-3} (left), *P* = 8.8 × 10^{-3} (right). For **b** and **c**, individual *P* values were derived from one-way ANOVA followed by Tukey's multiple comparisons test. **d**, Phosphorylation levels of p38 MAPK (p-p38) and JNK (pJNK) after stimulation of D1 mouse MSCs in suspension with TNF-α or IL-1β for 20 min. **P* = 3.7 × 10^{-2} via paired *t*-test. **e**, Dose–response curves of TNF-α to upregulate mRNA expression of collagenases in D1 mouse MSCs in soft or stiff bulk alginate-RGD hydrogels after 3-day treatment. Left: *Mmp13*: IC_{50} and maximum transcript levels for soft, 10.8 μM and 1.53, respectively; for stiff, 48.83 μM and 0.82, respectively. Right: *Mmp1a*: IC_{50} and maximum transcript levels for soft, 11.9 μM and 0.069, respectively; for stiff, 15.42 μM and 0.023, respectively. **P* = (0.3–4.9) × 10^{-2} (left), *P* = (0.9–4.8) × 10^{-2} (right) via two-way ANOVA followed by Bonferroni's multiple comparisons test. **f**, Phosphorylation levels of JNK after stimulation of D1 mouse MSCs in soft or stiff alginate-RGD gels with TNF-α for 20!min. **P* = 3.4×10^{-2} via paired *t*-test. The dotted lines in **d** and **f** indicate the normalized level of phosphorylated proteins without treatment with cytokines. For **b**–**f**, *n* = 3 independent experiments, each performed in three replicates; grey circles represent data points. All data are shown as mean ± s.e.m.

Author Manuscript Author Manuscript Author Manuscript Author Manuscript

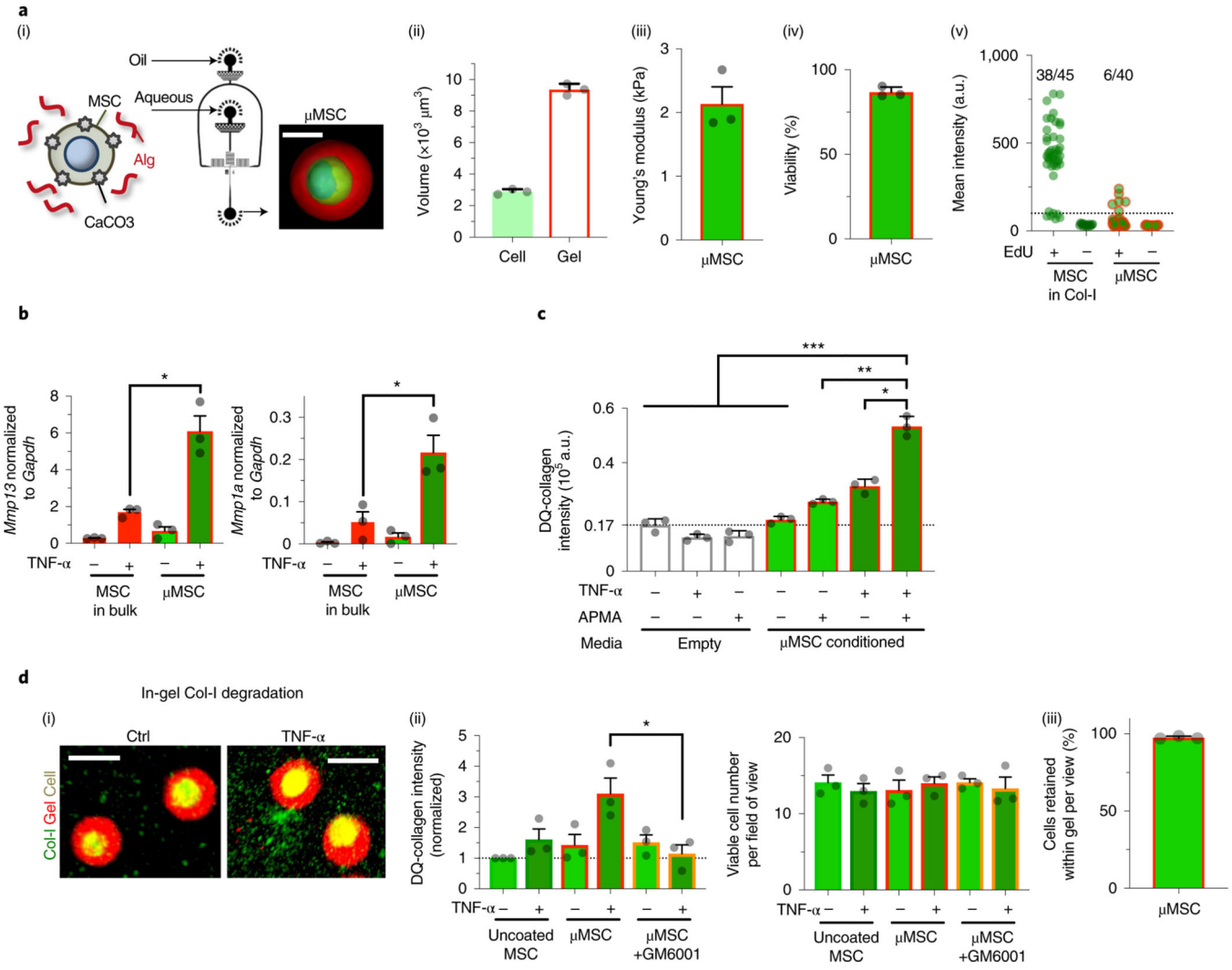

Fig. 2 |. Packaging chemomechanical cues into engineered gel coating for single mouse MSCs to enable paracrine matrix remodelling.

a, Characterization of gel-coated D1 mouse MSCs. (i) Schematic showing the droplet microfluidic approach to coat single MSCs in a thin layer of alginate (Alg) gels (μMSC) (Methods). Inset: representative confocal image of a gel-coated MSC after reconstruction (green, cytoplasm; blue, nucleus; red, alginate-rhodamine; scale bar, 10μm). (ii) Volume of cells (calcein) and gel coating (alginate-RGD with rhodamine) from confocal microscopy 6 h after encapsulation. $n = 3$ independent experiments, each averaged from seven gel-coated cells. (iii) Elasticity (Young's modulus, E) of the gel coating. $n = 3$ independent experiments, each averaged from five gel-coated cells. (iv) Percentage of viable gel-coated D1 mouse MSCs after 3 days in culture. $n = 3$ independent experiments, each performed in two replicates. (v) Incorporation of EdU by D1 mouse MSCs in collagen-I (Col-I) gel or gel-coated MSCs over 1 day in culture. The dotted line indicates a background signal measured in the absence of EdU. The values indicate the fractions of cells that incorporated EdU above the background level from the data pooled from 3 independent experiments. CaCO3, calcium carbonate nanoparticles; a.u., arbitrary units. **b**, Left: effects of TNF-α

Author Manuscript Author Manuscript Author Manuscript Author Manuscript

(100 ng ml^{-1}) on expression of *Mmp13*; and right: of *Mmp1a*, in D1 mouse MSCs in soft bulk gel or gel coating after 3-day treatment in culture. *$P = 4.5 \times 10^{-4}$ (left), $P = 5.9 \times 10^{-3}$ (right). **c**, Collagenase activity in the conditioned media. The media were collected from gel-coated MSCs (50,000 cells per 200 μl) ± TNF-α (100 ng ml^{-1}) for 3 days, followed by mixing with fluorogenic Col-I substrate (DQ-collagen, 100 μg ml^{-1}) ± latent MMP activator APMA (1 mM) and incubating for 1 day before readout. The dotted line indicates a background signal from a complete DMEM. *$P = 1.2 \times 10^{-7}$; **$P = 6.0 \times 10^{-9}$; ***$P = (0.4–3.7) \times 10^{-10}$. For **c** and **d**, $n = 3$ independent experiments, each performed in three replicates. **d**, Collagen degradation by embedded uncoated or gel-coated D1 mouse MSCs for 1 day in the presence of APMA. (i) Representative images. Scale bar, 20 μm. (ii) Quantification. Left: degraded DQ-collagen (green+) volume per field of view. GM6001 (10 μM): pan-MMP inhibitor. Each group was normalized to the uncoated MSC without TNF-α group.; *$P = 2.0 \times 10^{-2}$. Right: viable (calcein^{+}) cell number per field of view. $n = 3$ independent experiments, each averaged from three fields of view. (iii) Percentage of cells retained within gel coating after culturing for 3 days. $n = 3$ independent experiments, each averaged from five fields of view. Individual P values were derived from one-way ANOVA followed by Tukey's multiple comparisons test. Grey circles throughout represent data points. All data are shown as mean ± s.e.m.

Author Manuscript
Author Manuscript
Author Manuscript
Author Manuscript

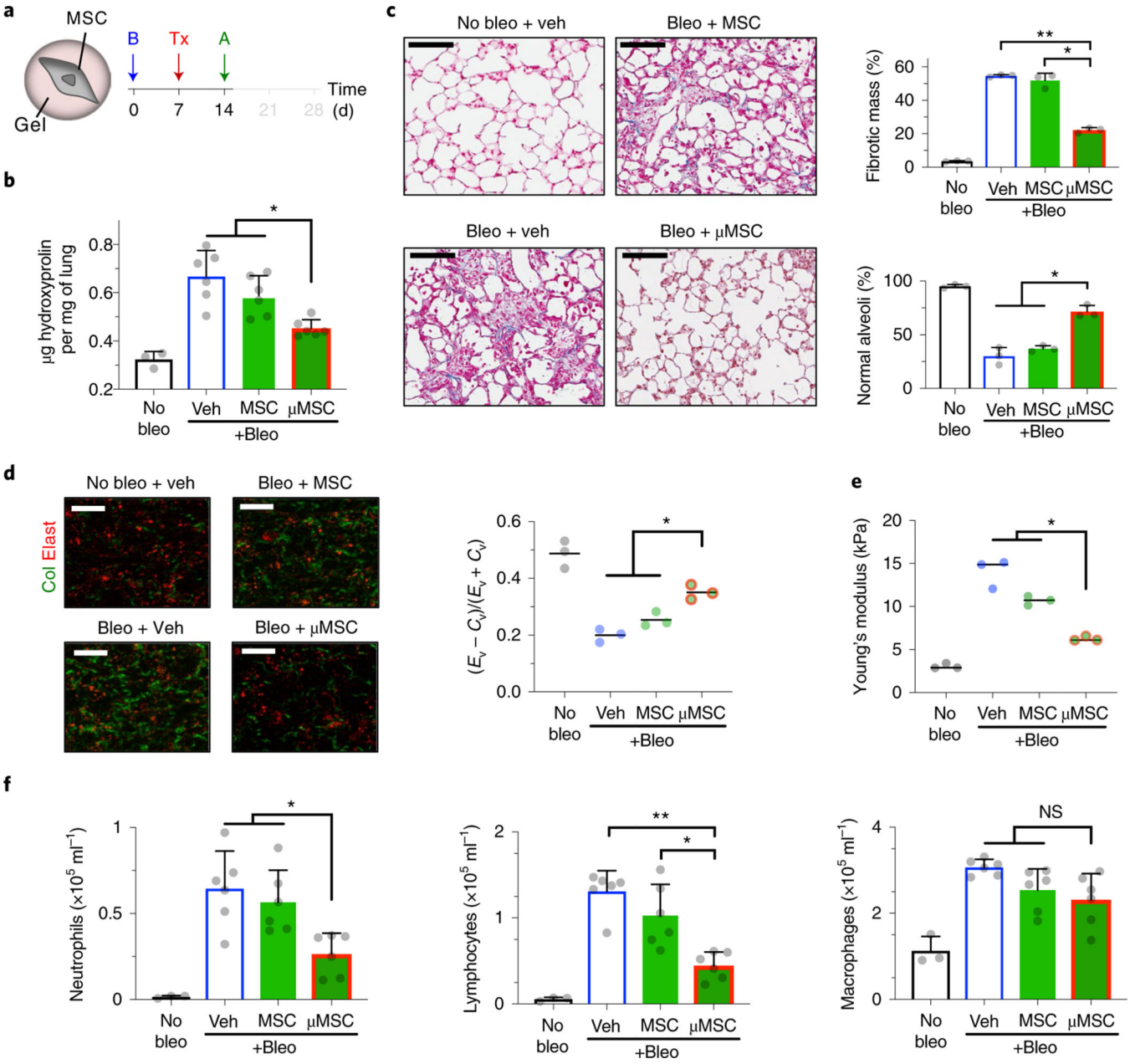

Fig. 3 |. Mouse MSCs in gel coating promote normal tissue remodelling after fibrotic lung injury.
a, Experimental design. B, bleomycin (bleo); Tx, treatment—vehicle (veh), uncoated D1 mouse MSCs or gel-coated MSCs (µMSCs); A, analysis. **b**, Hydroxyproline levels in lung tissue. $n = 3$ animals for no bleo and $n = 6$ for other groups. *$P = (1.8–4.1) \times 10^{-2}$. **c**, Histological evaluation of collagen deposition. Left: representative images from Masson's trichrome stain. Scale bar, 100µm. Top right: percent total fibrotic mass at low magnification. $n = 3$ animals per group, each data point averaged from three fields of view from three tissue sections of each animal. Bottom right: percent normal alveoli at high magnification. $n = 3$ animals per group, each data point averaged from nine fields of view from three tissue sections of each animal. *$P = 2.3 \times 10^{-2}$ (top right), $P = (8.2–9.9) \times 10^{-3}$

Author Manuscript Author Manuscript Author Manuscript Author Manuscript

(bottom right); $^{**}P = 2.1 \times 10^{-4}$ (top right). **d**, Parenchymal collagen and elastin levels. Left: representative images from two-photon microscopy. Scale bar, 20 μm. Right: elastin (E_v)-to-collagen (C_v) volume ratio index $(E_v - C_v)/(E_v + C_v)$. $n = 3$ animals per group, each data point averaged from three fields of view from a lung of each animal. $^{*}P = (0.7–4.2) \times 10^{-2}$. **e**, Microelasticity of lung tissue sections measured by atomic force microscopy. $n = 3$ animals per group, each data point averaged from 15 indentations of random regions from three tissue sections of each animal for no bleo, 30 indentations for other groups. $^{*}P = (0.4–4.8) \times 10^{-2}$. **f**, Left: quantification of neutrophils; middle: lymphocytes; and right: macrophages, in bronchoalveolar lavage fluid. n = same as **b**. $^{*}P = (3.0–4.8) \times 10^{-2}$ (left), $P = 4.4 \times 10^{-2}$ (middle); $^{**}P = 2.5 \times 10^{-4}$ (middle); NS, not significant; $P > 0.05$ (right). Individual P values were derived from one-way Welch ANOVA followed by Dunnett T3 multiple comparisons test. All data are shown as mean ± s.d.

Author Manuscript Author Manuscript Author Manuscript Author Manuscript

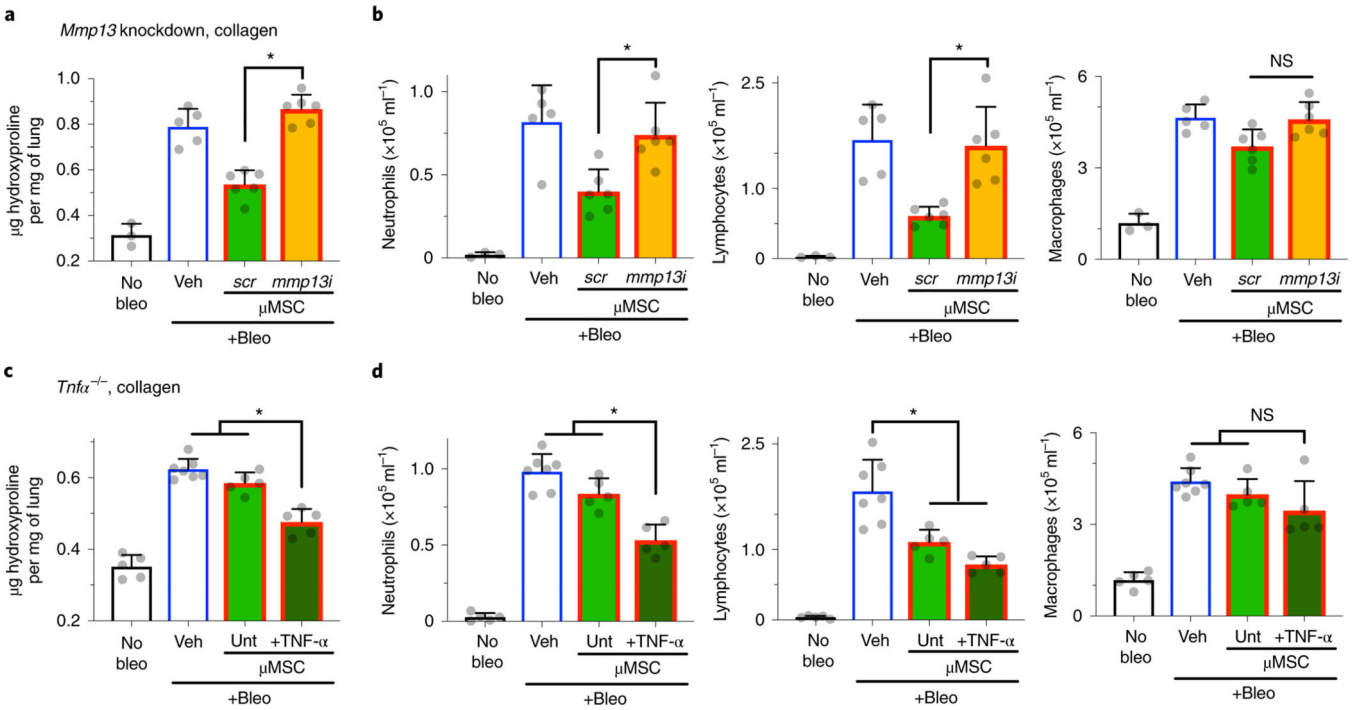

Fig. 4 |. Donor MMP13 and host TNF-α determine effects of gel-coated mouse MSCs on fibrotic lung injury.

a, Effects of *Mmp13* knockdown in gel-coated D1 mouse MSCs (µMSCs) on hydroxyproline levels in lung tissue. **b**, Left: quantification of neutrophils; middle: lymphocytes; and right: macrophages, in bronchoalveolar lavage fluid. For **a** and **b**, n = 3 animals for no bleomycin (bleo), n = 5 for bleo + vehicle (veh), and n = 6 for each of scrambled (*scr*) and *Mmp13* siRNA (*mmp13i*) µMSCs. *$P = 2.1 \times 10^{-5}$ (**a**); $P = 3.3 \times 10^{-2}$ (**b**, left), $P = 2.4 \times 10^{-2}$ (**b**, middle); NS, $P > 0.05$ (**b**, right). **c**, Effects of gel-coated D1 mouse MSCs on hydroxyproline levels in lung tissue of $Tnfa^{-/-}$ host animals. **d**, Left: quantification of neutrophils; middle: lymphocytes; and right: macrophages, in bronchoalveolar lavage fluid. For **c** and **d**, n = 5 animals for each of no bleo, bleo + untreated (unt) µMSCs, and bleo + TNF-α-treated µMSCs; and n = 7 for bleo + veh. *$P = (0.7–4.3) \times 10^{-3}$ (**c**), $P = (0.3–7.9) \times 10^{-3}$ (**d**, left), $P = (0.3–2.6) \times 10^{-2}$ (**d**, middle); NS, $P > 0.05$ (**d**, right). Individual P values were derived from one-way Welch ANOVA followed by Dunnett T3 multiple comparisons test. Data are shown as mean ± s.d.

Author Manuscript Author Manuscript Author Manuscript Author Manuscript

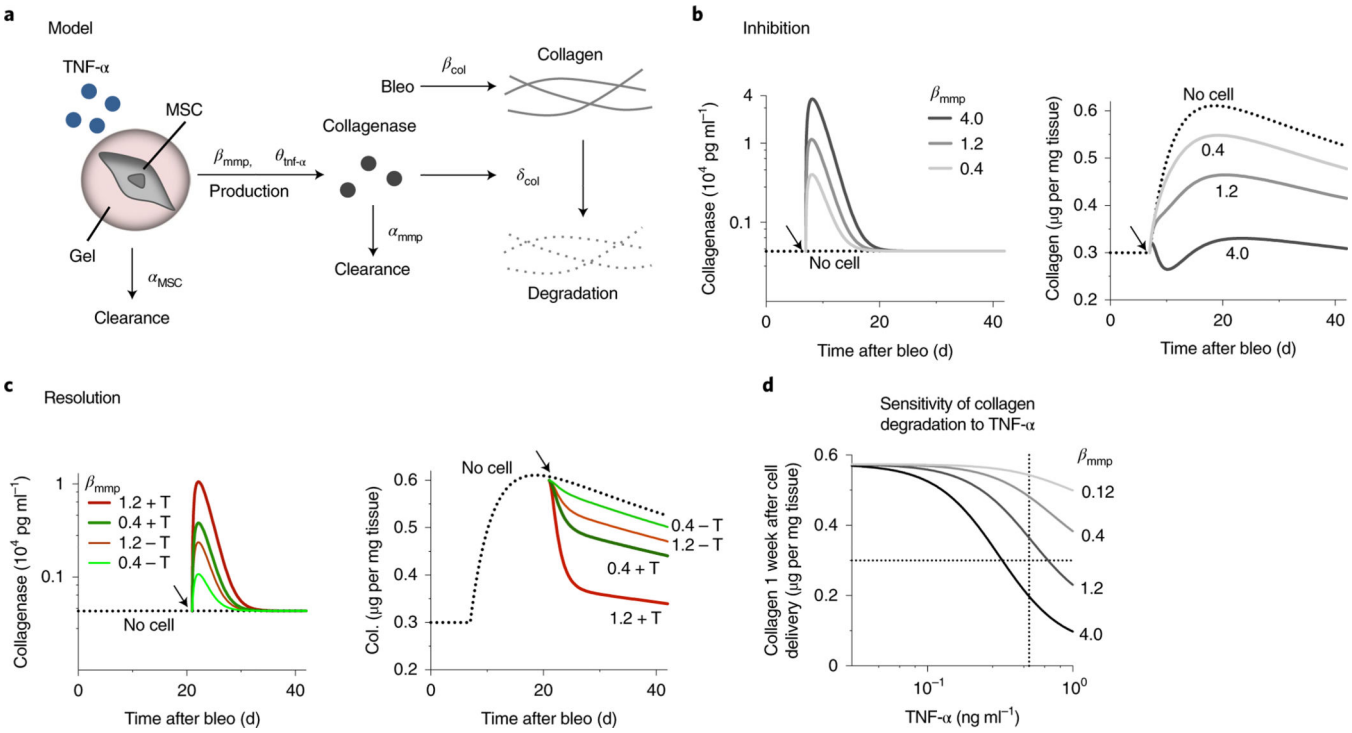

Fig. 5 |. Deterministic model predicts the effect of gel-coated MSCs on lung tissue collagen levels in different stages of bleomycin-induced injury.

a, Schematic depicting model of cell therapy to control host tissue collagen by delivering soluble interstitial collagenases (Supplementary Text). α_{MSC} is the clearance rate of donor MSCs. β_{mmp} (maximum production rate) and $\theta_{tnf\text{-}\alpha}$ (dose response of TNF-α) determine collagenase production by MSCs. Bleomycin (bleo) induces collagen production at the rate β_{col}, while collagenases degrade collagen based on the Michaelis–Menten kinetics, δ_{col}. Collagenases are cleared at the rate α_{mmp}. **b**, Left: simulation results for the effect of delivering MSCs 1 week after bleomycin (arrows) on collagenase; and right: on collagen levels in lung tissue, with β_{mmp} varying from 0.4 to 4.0. **c**, Left: simulation results for the effect of delivering MSCs 3 weeks after bleomycin (arrows) on collagenase; and right: on collagen levels in lung tissue, showing β_{mmp} = 0.4 and 1.2 without or with restoration of the maximum TNF-α level (±T) in the bleomycin-treated host. **d**, Simulation results for the sensitivity of collagen degradation to host TNF-α as a function of β_{mmp} when MSCs are delivered 3 weeks after bleomycin, followed by evaluation of tissue collagen 1 week after cell delivery. Vertical and horizontal dotted lines indicate the maximum level of TNF-α after a single dose of bleomycin and the physiological level of lung tissue collagen, respectively.

Author Manuscript Author Manuscript Author Manuscript Author Manuscript

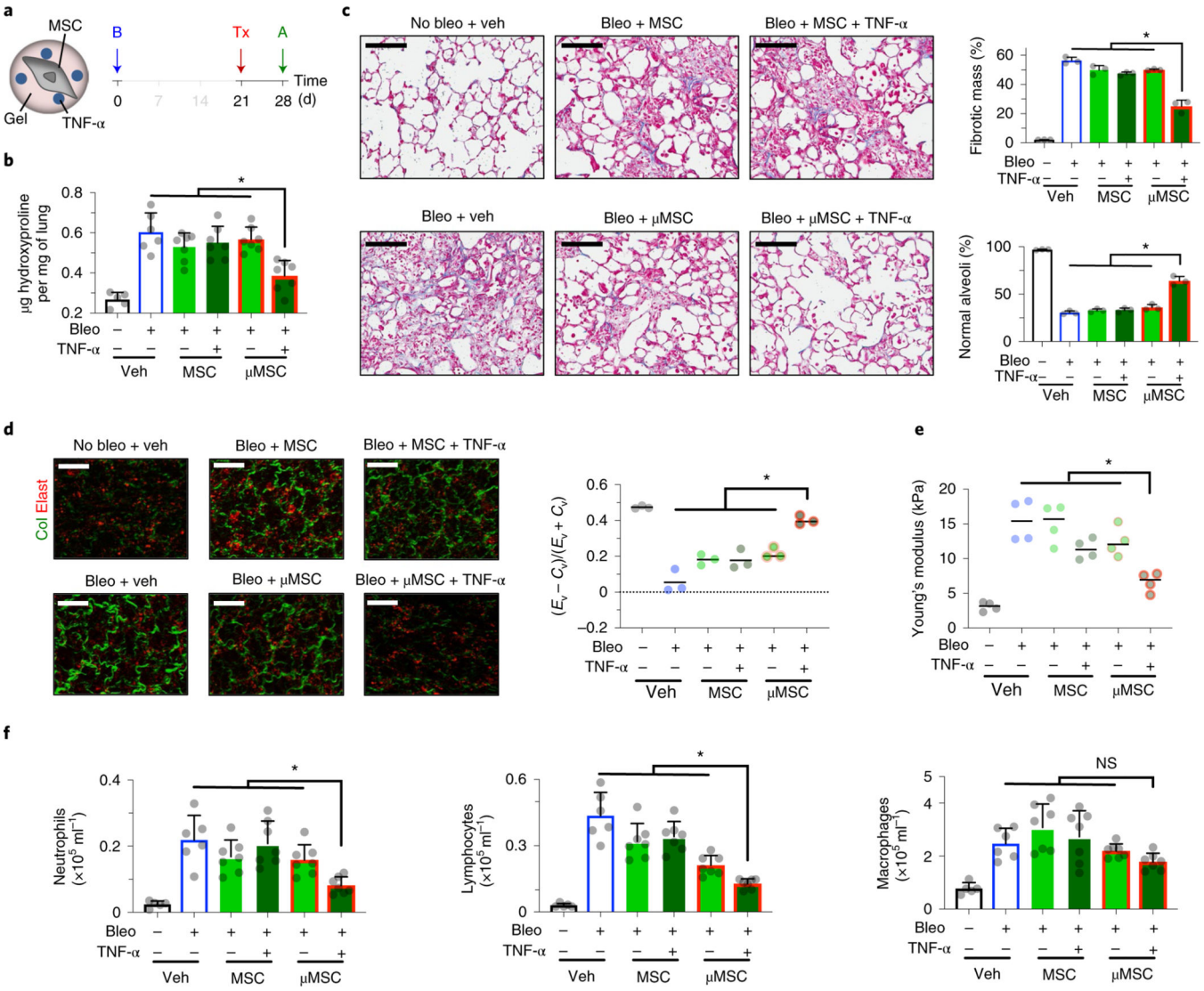

Fig. 6 |. Continuous presentation of recombinant TNF-α in gel coating enables mouse MSCs to accelerate the resolution of fibrotic phenotypes.

a, Experimental design. B, bleomycin (bleo); Tx, treatment—vehicle (veh), uncoated D1 mouse MSCs ± TNF-α or gel-coated MSCs (μMSCs) ± TNF-α; A, analysis. **b**, Hydroxyproline levels in lung tissue. $n = 5$ animals for no bleo, $n = 6$ for bleo + veh, and $n = 7$ for other groups. $*P = (0.6–4.2) \times 10^{-2}$. **c**, Histological evaluation of collagen deposition. Left: representative images from Masson's trichrome stain. Scale bar, 100μm. Top right: percent total fibrotic mass at low magnification. $n = 3$ animals per group, each data point averaged from three fields of view from three tissue sections of each animal. Bottom right: percent normal alveoli at high magnification. $n = 3$ animals per group, each data point averaged from nine fields of view from three tissue sections of each animal. $*P = (0.9–4.1) \times 10^{-2}$ (top right), $P = (2.8–4.0) \times 10^{-2}$ (bottom right). **d**, Parenchymal collagen and elastin levels. Left: representative images from two-photon microscopy. Scale bar, 20μm. Right: elastin (E_v)-to-collagen (C_v) volume ratio index $(E_v - C_v)/(E_v + C_v)$. $n = 3$ animals per group, each data point averaged from three fields of view from a lung

Author Manuscript Author Manuscript Author Manuscript Author Manuscript

of each animal. *P = (0.5–4.7) × 10^{-2}. **e**, Microelasticity of lung tissue sections measured by atomic force microscopy. n = 4 animals per group, each data point averaged from 15 indentations of random regions from three tissue sections of each animal for no bleo, 30 indentations for other groups. *P = (2.5–3.7) × 10^{-2}. **f**, Left: quantification of neutrophils; middle: lymphocytes; and right: macrophages, in bronchoalveolar lavage fluid. n = same as **b**; *P = (1.9–4.7) × 10^{-2} (left), P = (0.1–2.0) × 10^{-2} (middle); NS, P > 0.05 (right). Individual P values were derived from one-way Welch ANOVA followed by Dunnett T3 multiple comparisons test. Data are shown as mean ± s.d.